

On the interpretation of molecular photoexcitation with long and ultrashort laser pulses

Jiří Janoš,^{*,†,‡} Federica Agostini,[¶] Petr Slavíček,[†] and Basile F. E. Curchod^{*,‡}

[†]*Department of Physical Chemistry, University of Chemistry and Technology, Technická 5,
Prague 6, 166 28, Czech Republic*

[‡]*Centre for Computational Chemistry, School of Chemistry, University of Bristol, Bristol
BS8 1TS, United Kingdom*

[¶]*Sorbonne Université, CNRS, LCT UMR 7616, Paris 75005, France*

E-mail: jiri.janos@vscht.cz; basile.curchod@bristol.ac.uk

Abstract

Photoexcitation is an inherent part of any photochemical or spectroscopic experiment, yet its impact on the excited-state dynamics is often overlooked. However, it is the excited molecular state, built upon photoexcitation and shaped by the characteristics of the light source, that determines the fate of the excited molecule and its subsequent photochemical reactions. In this work, we investigate how excited molecular states are built by different laser pulses, leveraging two representations of the molecular wave function: Born–Huang expansion and exact factorization. We explore the generation of two limiting cases: a stationary molecular state with a long laser pulse and an electronic wave packet by an ultrashort (attosecond) laser pulse. The standard concepts of population transfer between electronic states, resonance condition, or sudden vertical excitation, inherent to the Born–Huang representation and used by chemists to approximate the impact of photoexcitation on molecular systems, are challenged by the exact factorization.

1 Introduction

The Grotthuss–Draper law, the first law of photochemistry, states that only the light absorbed by a molecular system can cause a photochemical reaction.^{1,2} While this law may appear trivial nowadays, it highlights the key impact of photoexcitation on the outcomes of photochemical reactions, and perhaps more importantly, on the molecular state such a photoexcitation generates.

The properties of the light source employed to excite a molecule—typically a laser pulse for time-resolved experiments or a continuous-wave (CW) laser for energy-resolved studies—may tune the precise *molecular state* generated upon photoexcitation.^{3–5} This molecular state, characterized by a (often time-dependent) molecular wave function depending on both electronic and nuclear degrees of freedom, is therefore carved by the driving light source. When an ultrashort (attosecond) laser pulse with a broad energy spectrum is sent on a molecule, the resulting molecular state upon photoexcitation is formed by a coherent superposition of

nuclear wave functions on multiple electronic states – a molecular state coined 'electronic wave packet' (where wave packet characterizes a coherent superposition of eigenstates, here electronic ones). Such an electronic wave packet exhibits an actual non-stationary electronic dynamics that lies at the heart of attochemistry. Extending the laser pulse to a few tens of femtoseconds reduces the span of its energy spectrum, meaning that its application to a molecular system will usually target only a single electronic state, yet the molecular state formed can still be composed by a coherent superposition of eigenstates, this time of vibrational (nuclear) eigenstates. Such molecular states are called nuclear or vibrational wave packets. Vibrational wave packets feature nearly classical nuclear dynamics and have been the central quantity of interest in femtochemistry. Finally, long CW laser pulses have a well-defined frequency, which may target only a single vibrational state of a given electronic excited state, forming then a stationary molecular state called a vibronic state. It is often in the context of a photoexcitation triggered by a long CW laser that various well-known concepts in photochemistry are introduced, e.g., Franck-Condon factors, resonance condition, or the Franck-Condon principle, which states that an electronic transition occurs, to a good approximation, without changes in the position of the nuclei of a molecule.^{3,6,7}

This brief survey of photoexcitation hopefully highlights the key importance of the photoexcitation process in creating a new molecular state, whose properties may alter outcomes of photochemical reactions. Yet, it is central to realize that the perspective presented above and its vocabulary—electronic and vibrational eigenstates, wave packets—belong to a specific representation of the molecular wave function called Born–Huang (BH).⁸ It is within this BH representation that a molecular wave function can be defined as a linear combination of static electronic states multiplied by time-dependent nuclear amplitudes, yielding a picture of nuclei evolving on static electronic potential energy surfaces and transferring between them.^{9–11} The BH representation is, however, not the only possible representation for the molecular wave function. An alternative and equally exact representation is the so-

called exact factorization (EF), which represents the molecular state as a single product of a nuclear state and an electronic state, both time-dependent.^{12,13} Within the single product representation offered by EF, the vocabulary and concepts dear to the photochemists—static electronic states and static potential energy surfaces guiding time-dependent nuclear wave functions—do not exist anymore.^{11,14} As such, EF depicts the building of excited molecular states by photoexcitation in a fundamentally different and truly unconventional picture. Historically, shifting perspectives on established concepts in quantum mechanics often led to deeper understanding and the development of novel practical approaches, as exemplified by the impact of path integrals or Bohmian dynamics. The perspective provided by EF on the specific process of photoexcitation has remained unexplored to date.

The central questions of this work are therefore: can switching to the EF representation of the molecular wave function bring a new picture and understanding of molecular photoexcitation? Does it challenge traditional textbook concepts that belong solely to the BH representation? Can EF offer a new route for simulating molecular photoexcitation?

To address these questions, we developed a complete model for the photoexcitation of hydroxyl radical, which allowed us to explore distinct photoexcitation scenarios: a long 100-fs laser pulse forming a stationary molecular state and a 1-fs laser pulse creating an electronic wave packet. The long 100-fs pulse depicts the gradual build-up of the stationary molecular state, whereas the short 1-fs laser pulse reveals the sudden formation of an electronic wave packet – a scenario common in attochemistry.

Our results question our understanding of photoexcitation rooted in the BH representation, revealing a striking conceptual difference between the two representations of molecular states: *(i)* a population transfer between stationary states in the BH expansion can be equally viewed as tunnelling in EF, *(ii)* the abstract (and somewhat hidden) implications of a vertical excitation and resonance condition, connected to the Franck–Condon principle, are highlighted by the EF and clarified by its formalism, and *(iii)* the EF permits to demonstrate

pitfalls in simulating photoexcitation with a truncated basis (Hilbert space) that would emerge from a BH understanding of photoexcitation.

The paper is organized as follows. Section 2 offers a pedagogical introduction to the theoretical background behind the BH and EF representations. A description of the hydroxyl radical model and the methodology applied in this work is detailed in Section 3. We then present our results and discuss their implications in Section 4, before drawing our conclusions and assessing their impact on the field of photochemistry in Section 5.

2 Theoretical background

In this Section, we begin by introducing the concept of the molecular wave function, representing the molecular state discussed in the Introduction, and the corresponding time-dependent Schrödinger equation. We follow by discussing two different representations – the BH expansion and EF of the molecular wave function – along with their equations of motion.

2.1 Molecular wave function and Born–Oppenheimer approximation

The object of interest throughout this Section is the molecular wave function, Ψ , which contains the complete information about the molecular state. The molecular wave function is, in the position representation, a complex function of the positions of all the particles composing a molecular system and time t . Although all the particles are treated equally in quantum mechanics, we tend to formally distinguish them by marking the positions of lighter electrons with \mathbf{r} and heavier nuclei with \mathbf{R} . Using this notation, the molecular wave function is then written in the position representation as $\Psi(\mathbf{r}, \mathbf{R}; t)$. Note that since the dependence on time in the molecular wave function is parametric in non-relativistic quantum mechanics, we separate it (and any other parametric dependence in any other wave function) by a semicolon from the remaining physical variables for wave functions.

The time evolution of $\Psi(\mathbf{r}, \mathbf{R}; t)$ in a non-relativistic framework is governed by the time-dependent Schrödinger equation,

$$i\hbar \frac{\partial}{\partial t} \Psi(\mathbf{r}, \mathbf{R}; t) = \hat{H}(\mathbf{r}, \mathbf{R}, t) \Psi(\mathbf{r}, \mathbf{R}; t), \quad (1)$$

where $\hat{H}(\mathbf{r}, \mathbf{R}, t)$ is the molecular Hamiltonian defined as

$$\hat{H}(\mathbf{r}, \mathbf{R}, t) = \hat{T}_n + \hat{T}_e + \hat{V}_{nn}(\mathbf{R}) + \hat{V}_{en}(\mathbf{r}, \mathbf{R}) + \hat{V}_{ee}(\mathbf{r}) + \hat{V}_{int}(\mathbf{r}, \mathbf{R}, t). \quad (2)$$

The molecular Hamiltonian contains the following terms: kinetic energy operators for nuclei (\hat{T}_n) and electrons (\hat{T}_e), Coulomb interactions between electrons and nuclei [$\hat{V}_{nn}(\mathbf{R})$, $\hat{V}_{en}(\mathbf{r}, \mathbf{R})$, and $\hat{V}_{ee}(\mathbf{r})$], and a time-dependent external interaction term [$\hat{V}_{int}(\mathbf{r}, \mathbf{R}, t)$]. The external interaction—here, the electromagnetic field of a laser pulse for our interest in photoexcitation—can affect both electrons and nuclei: $\hat{V}_{int}(\mathbf{r}, \mathbf{R}, t) = \hat{V}_{int}^e(\mathbf{r}, t) + \hat{V}_{int}^n(\mathbf{R}, t)$. We will use this decomposition later when we discuss the equations of motion related to EF.

To alleviate the complexity related to the full molecular wave function, a suitable representation decomposing $\Psi(\mathbf{r}, \mathbf{R}; t)$ into quantities related to the electrons and the nuclei is desirable. The first and seminal step in this direction was made by Born and Oppenheimer,¹⁵ who realized that electrons are much lighter than nuclei and can adapt to nuclear motion almost instantaneously under certain conditions. Formulating this assumption mathematically is equivalent as to say that, independently of the nuclear motion, electrons always remain adiabatically in a single electronic state; in other words, the total molecular wave function can be written as a product of a time-dependent nuclear wave function $\chi(\mathbf{R}; t)$ and a time-independent electronic wave function $\Phi(\mathbf{r}; \mathbf{R})$,

$$\Psi(\mathbf{r}, \mathbf{R}; t) \approx \chi(\mathbf{R}; t) \Phi(\mathbf{r}; \mathbf{R}). \quad (3)$$

The electronic wave function depends parametrically on the nuclear positions \mathbf{R} , which gives its squared modulus a conditional probability nature, reflecting the assumption that the electrons can adapt to the nuclei instantaneously. The advantage of Eq. (3) is that it separates the molecular wave function into two wave functions—one for nuclei and one for electrons—which can be analyzed (and visualized) separately.

Where does the electronic wave function in Eq. (3) come from? The electronic wave function can be taken as an eigenstate of the electronic subsystem, i.e., a solution of the time-independent electronic Schrödinger equation

$$\hat{H}_{\text{el}}(\mathbf{r}, \mathbf{R})\Phi(\mathbf{r}; \mathbf{R}) = \varepsilon(\mathbf{R})\Phi(\mathbf{r}; \mathbf{R}), \quad (4)$$

where the electronic subsystem is defined by the electronic or Born–Oppenheimer Hamiltonian $\hat{H}_{\text{el}} = \hat{T}_{\text{e}} + \hat{V}_{\text{nn}}(\mathbf{R}) + \hat{V}_{\text{en}}(\mathbf{r}, \mathbf{R}) + \hat{V}_{\text{ee}}(\mathbf{r})$. The quantity $\varepsilon(\mathbf{R})$ is then the electronic energy, forming a potential energy surface for the nuclei when Eq.(4) is solved for all possible nuclear configurations \mathbf{R} .¹⁶ The Born–Oppenheimer molecular wave function is often expressed for the ground electronic state, i.e., $\Phi(\mathbf{r}; \mathbf{R}) \equiv \Phi_0(\mathbf{r}; \mathbf{R})$ and $\varepsilon(\mathbf{R}) \equiv \varepsilon_0(\mathbf{R})$. However, we can write this approximation to the molecular wave function for any electronic states, and we label these eigenstates by J : $\Phi_J(\mathbf{r}; \mathbf{R})$ and $\varepsilon_J(\mathbf{R})$.

The product form in Eq. (3) is, however, only an approximation as such a simple product is only able to account for the full complexity of the molecular wave function under certain conditions. Hence, Eq. (3) is known as the *Born–Oppenheimer approximation* (BOA). The failures of BOA are well known: its simple product cannot describe nonadiabatic phenomena, that is, processes involving the coupling between nuclear and electronic motion. In addition, the simple BOA molecular wave function does not allow a rigorous description of a photoexcitation between electronic states. To create an in-principle exact representation for the molecular wave function, one needs to make a step beyond BOA.

2.2 Born–Huang expansion of the molecular wave function

The most straightforward way to correct the BOA wave function towards an exact representation relies on the property that the electronic Hamiltonian generates a set of orthonormal electronic eigenstates. The molecular wave function can be expanded in this basis with expansion coefficients $\chi(\mathbf{R}; t)$ depending on the remaining variables \mathbf{R} and t . Mathematically speaking, we can suggest the following Ansatz,

$$\Psi(\mathbf{r}, \mathbf{R}; t) = \sum_J \chi_J(\mathbf{R}; t) \Phi_J(\mathbf{r}; \mathbf{R}), \quad (5)$$

which implies that we can form Born–Oppenheimer products (3) for each electronic state and sum them up. This Ansatz is known as the *Born–Huang expansion* (BH) of the molecular wave function.⁸ In the following, we summarize the main aspects of the BH expansion which are detailed in the following references: 11,17–19.

As stated above, the electronic states are the eigenstates of the electronic Hamiltonian $\hat{H}_{\text{el}}(\mathbf{r}, \mathbf{R})$; hence, they are obtained from the time-independent Schrödinger equation,

$$\hat{H}_{\text{el}}(\mathbf{r}, \mathbf{R}) \Phi_J(\mathbf{r}; \mathbf{R}) = \varepsilon_J(\mathbf{R}) \Phi_J(\mathbf{r}; \mathbf{R}), \quad (6)$$

where $\varepsilon_J(\mathbf{R})$ now represents an infinite set of electronic energies corresponding to different electronic states J . As such, electronic wave functions and electronic energies (that is, potential energy surfaces) do not depend on time explicitly and can be precomputed before any dynamical simulation. This stationary electronic basis is the advantage of the BH expansion as it allows us to plot the potential energy landscape of any molecule and use it to infer possible dynamical scenarios.

Plugging the BH expansion [Eq. (5)] into the time-dependent Schrödinger equation [Eq. (1)]

yields a set of coupled equations of motion for the nuclear amplitudes,

$$i\hbar \frac{\partial}{\partial t} \chi_J(\mathbf{R}; t) = \sum_{K=1}^{\infty} [(\hat{T}_n + \varepsilon_K(\mathbf{R})) \delta_{JK} + \hat{D}_{JK}(\mathbf{R}) + \hat{V}_{\text{int},JK}(\mathbf{R}, t)] \chi_K(\mathbf{R}; t), \quad (7)$$

where $\hat{T}_n = -\sum_{\alpha=1}^{N_n} \frac{\hbar^2 \nabla_{\alpha}^2}{2M_{\alpha}}$ is the nuclear kinetic energy operator with N_n being the number of nuclei and α their index, \hat{D}_{JK} are the so-called nonadiabatic coupling terms,

$$\hat{D}_{JK}(\mathbf{R}) = -\sum_{\alpha=1}^{N_n} \frac{\hbar^2}{2M_{\alpha}} [\langle \Phi_J(\mathbf{R}) | \nabla_{\alpha}^2 | \Phi_K(\mathbf{R}) \rangle_r + 2\langle \Phi_J(\mathbf{R}) | \nabla_{\alpha} \Phi_K(\mathbf{R}) \rangle_r \cdot \nabla_{\alpha}] ,^a \quad (8)$$

and $\hat{V}_{\text{int},JK}$ represents a coupling term with the external potential,

$$\hat{V}_{\text{int},JK}(\mathbf{R}, t) = \langle \Phi_J(\mathbf{R}) | \hat{V}_{\text{int}}(\mathbf{R}, t) | \Phi_K(\mathbf{R}) \rangle_r . \quad (9)$$

Solving these coupled equations requires prior knowledge of the electronic wave functions (for the nonadiabatic coupling and interaction terms) together with the electronic energies. Hence, the electronic time-independent Schrödinger equation [Eq. (6)] must be solved before the nuclear propagation, in principle for any possible nuclear configuration.

The dynamics of a molecular system based on Eq. (7) reads as follows: the nuclear amplitudes $\chi_J(\mathbf{R}; t)$ evolve on their respective potential energy surfaces $\varepsilon_J(\mathbf{R})$, whilst being mutually coupled by the nonadiabatic couplings $\hat{D}_{JK}(\mathbf{R})$ and interaction terms $\hat{V}_{\text{int},JK}(\mathbf{R}, t)$. Due to these couplings, nuclear amplitude can be transferred from one electronic state to another and, as such, implicitly reflect the electron dynamics during nonadiabatic events (or photoexcitation). Hence, the electronic dynamics is encoded in the nuclear amplitudes as well as the nuclear dynamics within the BH representation. For example, a purely electronic exci-

^aWe adapt the bra-ket notation where $\langle \cdot \rangle_r$ indicates the inner product taken over the electronic degrees of freedom. Note that the kets $|\Phi_J(\mathbf{R})\rangle$ or bras $\langle \Phi_J(\mathbf{R})|$ carry no explicit dependence on the electronic coordinates \mathbf{r} as they denote electronic states, not coordinate-space functions. Their dependence on the nuclear coordinates \mathbf{R} (and possibly on time t) is purely parametric.

tation triggered by $\hat{V}_{\text{int}}^e(\mathbf{r}, t)$ is described at the level of the nuclear amplitudes as a transfer of amplitude between different electronic states. The complexity associated with the expansion coefficients, i.e., the nuclear amplitudes, and their dynamics in the BH representation explains the rather challenging interpretation of the resulting equations of motion.

Finally, we note that the full set of electronic states can also be transformed to a different basis, such as a diabatic basis.²⁰ Diabatic basis might be more suitable for different kinds of applications, yet the conceptual picture remains the same.

2.3 Exact factorization of the molecular wave function

An alternative approach exists to offer an exact representation of the molecular wave function whilst retaining the appealing single-product form of BOA. The exact factorization (EF) of the molecular wave function proposes to renounce the assumption that electrons instantaneously adapt to the nuclear motion by using a single, yet time-dependent electronic wave function which is still parametrically dependent on the nuclear positions. The single-product form of the molecular wave function offered by the EF reads

$$\Psi(\mathbf{r}, \mathbf{R}; t) = \chi(\mathbf{R}; t)\Phi(\mathbf{r}; t, \mathbf{R}). \quad (10)$$

In this representation, it is no longer assumed that the electronic wave function is an eigenstate of the electronic Hamiltonian [as in BH, Eq. (6)]. As such, the single-product form of the molecular wave function is not uniquely defined within the EF: if we were to multiply $\chi(\mathbf{R}; t)$ by some nonzero factor and divide $\Phi(\mathbf{r}; t, \mathbf{R})$ by the same factor, we would obtain the same overall molecular wave function $\Psi(\mathbf{r}, \mathbf{R}; t)$.^b This ambiguity in the single-product Ansatz

^bIn contrast, the BH expansion is uniquely defined since the electronic states are taken as an orthonormal basis set, and are uniquely defined only up a sign if they are real.

[Eq. (10)] is naturally removed by the partial normalization condition (PNC)

$$\langle \Phi(t, \mathbf{R}) | \Phi(t, \mathbf{R}) \rangle_r = 1 \quad \forall \mathbf{R}, t. \quad (11)$$

which allows us to identify the electronic wave function as a proper conditional amplitude, whose squared modulus yields a normalized conditional probability density. PNC makes the product in Eq. (10) unique up to a gauge, which will be discussed later. Moreover, PNC gives $\chi(\mathbf{R}; t)$ the meaning of a true nuclear wave function by reproducing the exact nuclear density: $|\chi(\mathbf{R}; t)|^2 = \int |\Psi(\mathbf{r}, \mathbf{R}; t)|^2 d\mathbf{r}$. Formally, it is the combination of the Ansatz for the molecular wave function [Eq. (10)] together with PNC that strictly defines the *exact factorization* of the molecular wave function.

The equations of motion in EF are obtained by inserting the EF Ansatz into the time-dependent Schrödinger equation (1) and imposing PNC, which leads to a set of two coupled time-dependent equations.^{13,21} The equation of motion for the electronic wave function reads

$$i\hbar \frac{\partial}{\partial t} \Phi(\mathbf{r}; t, \mathbf{R}) = [\hat{H}_{\text{el}}(\mathbf{R}, t) + \hat{V}_{\text{int}}^e(\mathbf{r}, t) + \hat{U}_{\text{en}}[\chi, \Phi](\mathbf{R}, t) - \varepsilon(\mathbf{R}, t)] \Phi(\mathbf{r}; t, \mathbf{R}), \quad (12)$$

while the equation of motion for the nuclear wave function is

$$i\hbar \frac{\partial}{\partial t} \chi(\mathbf{R}; t) = \left[\sum_{\alpha=1}^{N_n} \frac{[-i\hbar \nabla_{\alpha} + \mathbf{A}_{\alpha}(\mathbf{R}, t)]^2}{2M_{\alpha}} + \hat{V}_{\text{int}}^n(\mathbf{R}, t) + \varepsilon(\mathbf{R}, t) \right] \chi(\mathbf{R}; t). \quad (13)$$

Three new quantities were introduced in the previous equations, expressing the coupling between electrons and nuclei: the time-dependent vector potential $\mathbf{A}(\mathbf{R}, t)$, the time-dependent potential energy surface $\varepsilon(\mathbf{R}, t)$, and the electron-nuclear coupling operator $\hat{U}_{\text{en}}[\chi, \Phi](\mathbf{R}, t)$. In the following, we will briefly discuss the interpretation of these three terms and the EF equations of motion. A detailed derivation and analysis of the EF equations can be found in the literature.^{13,21–24}

The time-dependent vector potential (TDVP) for nucleus α is defined as

$$\mathbf{A}_\alpha(\mathbf{R}, t) = -i\hbar \langle \Phi(t, \mathbf{R}) | \nabla_\alpha \Phi(t, \mathbf{R}) \rangle_r \quad (14)$$

and bears a character of a nuclear momentum field. In EF, the total nuclear momentum is a sum of two contributions: from the nuclear wave function $\chi(\mathbf{R}; t)$ and from TDVP. Hence, TDVP captures the not-irrotational part of nuclear momentum that is missing in the (curl-free component carried by the) nuclear wave function $\chi(\mathbf{R}; t)$, but is encoded in the electronic wave function $\Phi(\mathbf{r}; t, \mathbf{R})$ due to the single-product ansatz of the EF.

The time-dependent potential energy surface (TD PES) appearing in both electronic and nuclear equations of motion is defined as

$$\varepsilon(\mathbf{R}, t) = \langle \Phi(t, \mathbf{R}) | \hat{H}_{\text{el}}(\mathbf{R}, t) + \hat{V}_{\text{int}}^e(t) + \sum_{\alpha=1}^{N_n} \frac{[-i\hbar \nabla_\alpha - \mathbf{A}_\alpha(\mathbf{R}, t)]^2}{2M_\alpha} - i\hbar \frac{\partial}{\partial t} | \Phi(t, \mathbf{R}) \rangle_r. \quad (15)$$

TD PES consists of four different terms and provides an exact time-dependent generalization of the Born–Oppenheimer potential energy surface. The meaning of the first two terms is intuitive: the electronic Hamiltonian term creates a mean-field potential energy surface similar to that obtained in Ehrenfest dynamics (but with the EF electronic wave function), while the electronic interaction term accounts for the response of the electrons to the external interaction. The meaning of the remaining two terms is more elusive, but they introduce the entanglement between electrons and nuclei missing from the mean-field Ehrenfest time-dependent potential energy surface.²⁵

Finally, the electron-nuclear coupling operator is given by

$$\hat{U}_{\text{en}}[\chi, \Phi](\mathbf{R}, t) = \sum_{\alpha=1}^{N_n} \frac{1}{M_\alpha} \left[\frac{[-i\hbar \nabla_\alpha - \mathbf{A}_\alpha(\mathbf{R}, t)]^2}{2} + \left(\frac{-i\hbar \nabla_\alpha \chi(\mathbf{R}; t)}{\chi(\mathbf{R}; t)} + \mathbf{A}_\alpha(\mathbf{R}, t) \right) \cdot (-i\hbar \nabla_\alpha - \mathbf{A}_\alpha(\mathbf{R}, t)) \right]. \quad (16)$$

Note that, unlike TDVP and TDPES which depend solely on the electronic wave function, the electron-nuclear coupling operator depends on both the nuclear and electronic wave functions. As such, this quantity brings a coupling to the nuclei in the equation of motion for the electronic wave function [Eq. (12)], leading to its name: the electron-nuclear coupling operator. Analogously to TDVP, \hat{U}_{en} can be related to a contribution to the total nuclear kinetic energy that is missing in the nuclear wave function $\chi(\mathbf{R}; t)$ (see Ref. 13 for details).

The three quantities described above—TDVP, TDPES, and the electron-nuclear coupling operator—are responsible for the coupling between electrons and nuclei within the EF framework. While the electron-nuclear coupling ties the electronic equation of motion [Eq. (12)] to that for the nuclei [Eq. (13)], TDVP and TDPES couple the nuclei [Eq. (13)] to the electrons [Eq. (12)]. Hence, the TDVP and TDPES are powerful interpretative tools in nonadiabatic quantum molecular dynamics as they unravel the electronic effects on nuclei.

Let us now inspect the electronic and nuclear equations of motion [Eq. (12) and Eq. (13)]. The electronic equation of motion is, due to its non-Hermitian Hamiltonian, a non-unitary Schrödinger-like equation, yet still preserving the norm.²⁶ This equation of motion is also non-linear due to the electron-nuclear coupling operator \hat{U}_{en} , making any numerical solution of this equation challenging.^{27,28} The interaction of the electronic wave function with an external potential (e.g., the electric field of a laser pulse) appears in the electronic equation of motion both directly via the interaction operator $\hat{V}_{\text{int}}^e(\mathbf{r}, t)$ and indirectly via the TDPES. Thus, the electronic response to the field is directly contained in the electronic equation of motion, unlike in the BH representation. On the other hand, the equation of motion for the nuclear wave function satisfies a standard time-dependent Schrödinger equation with a time-dependent scalar $[\varepsilon(\mathbf{R}, t)]$ and vector potentials $[\mathbf{A}(\mathbf{R}, t)]$, which couple the nuclei to the electrons.²⁶ The interpretation of Eq. (13) is straightforward: the nuclei evolve on the TDPES under the influence of an additional momentum field provided by TDVP. This interpretation makes both the TDPES and the TDVP key interpretative tools for the coupled-

electron-nuclear dynamics. The nuclei are also directly coupled to the external potential via the $\hat{V}_{\text{int}}^n(\mathbf{R}, t)$ operator. Note that the electronic response to the external potential manifests purely through TDPES and TDVP.

Finally, we comment on the gauge freedom inherent to the EF framework. The product form in Eq. (10) is still not uniquely defined, even with the introduction of the PNC.¹³ The product can be multiplied and divided by a phase factor $e^{i\theta(\mathbf{R}, t)/\hbar}$ without altering the total wave function or any observables. The uniqueness of the product form of the molecular wave function within the EF is then guaranteed by fixing the gauge [either by directly selecting a functional form for $\theta(\mathbf{R}, t)$ or by indirectly imposing a condition on the gauge potentials]. Multiple gauges have been introduced in the EF.²⁴ The most common gauge sets the phase of $\chi(\mathbf{R}; t)$ to zero, where all the nuclear momentum is thus contained in TDVP. Another common gauge, which is only possible in one-dimensional systems,¹⁴ sets TDVP to zero and contains all electronic effects in TDPES.²²

2.3.1 Exact factorization for one nuclear degree of freedom

In our specific case of a one-dimensional OH radical model, the nuclear equation (13) of EF further simplifies. Firstly, the laser field polarization is selected such that the nuclear interaction term $\hat{V}_{\text{int}}^n(R, t)$ disappears and the laser field interacts directly only with the electronic subsystem (see Sec. 3.1). Note that since the OH radical is a one-dimensional system, we work with a single nuclear variable R . Secondly, we employ the gauge setting TDVP to zero, as mentioned above. Together, these two assumptions lead to a simpler nuclear equation of motion,

$$i\hbar \frac{\partial}{\partial t} \chi(R; t) = [\hat{T}_n + \varepsilon(R, t)] \chi(R; t), \quad (17)$$

where the TDPES completely governs the nuclear dynamics. Hence, the TDPES constitutes a suitable tool for analyzing and interpreting nuclear dynamics.

In multidimensional systems, the TDVP cannot be generally gauged away¹⁴ and comes along with TDPEs in analysis. To highlight that our conclusions are not restricted only to one-dimensional systems by our selection of gauge but extend also to molecular systems, we provide results with a gauge setting the nuclear phase to zero as mentioned above in the Supporting Information.

3 Methods

In this Section, we detail the methodology and the model system used in this work. We begin by defining our model system, inspired by the hydroxyl radical, and follow with a discussion of the two applied laser pulses. Finally, we provide details about our quantum dynamics calculations and the codes used.

3.1 Model system inspired by hydroxyl radical

The model employed in this work is based on a two-state model of hydroxyl (OH) radical introduced by Korolkov and Paramonov in 1998.²⁹ This model considers the lowest two diabatic electronic states of the OH radical, $X^2\Pi$ (ignoring its double degeneracy) and $A^2\Sigma^+$, both being bound states.

Since we target complex photoexcitation processes, we extended this model by including two more diabatic states, $1^2\Sigma^-$ and $1^2\Delta$, which both exhibit a dissociative character. Following Korolkov and Paramonov, we ignore the electronic states of higher spin multiplicity, as the spin-orbit coupling would facilitate a population transfer on a much longer (picosecond) timescale.²⁹ It is this extended OH radical model that we discuss in detail below, with additional validations and its relation to the original model of Korolkov and Paramonov detailed in the Supporting Information. We stress at this point that the present model is not *per se* intended for a quantitative modelling of the OH radical, but it rather targets a qualitative

exploration of photoexcitation processes of this molecule.

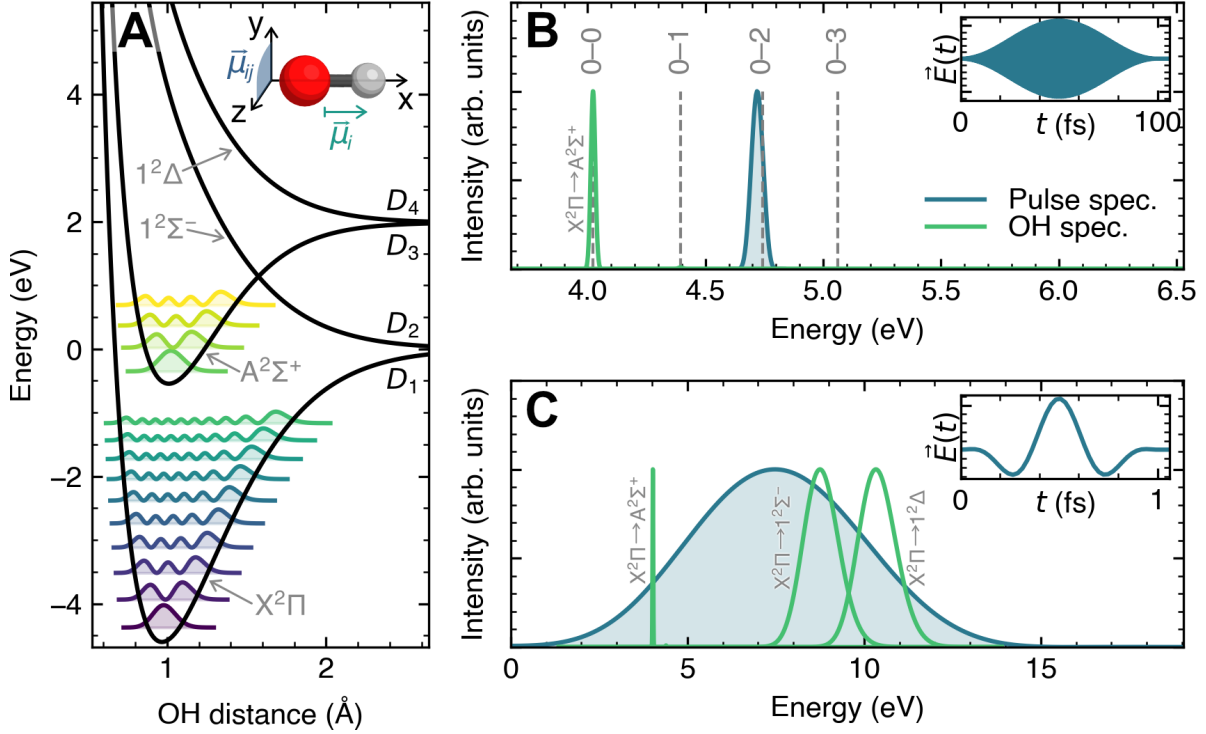


Figure 1: **A**: Potential energy curves of the OH radical model with the relevant vibrational eigenstates of the lowest two diabatic states. The diabatic state labels ($X^2\Pi$, $A^2\Sigma^+$, $1^2\Sigma^-$, $1^2\Delta$) are depicted together with adiabatic state labels (D_1 , D_2 , D_3 , D_4). The inset portrays the molecule and a schematic depiction of the dipole and transition dipole moments. **B**: Zoom on the region of the absorption spectrum of the OH radical concerned with the $X^2\Pi \rightarrow A^2\Sigma^+$ electronic transition, depicted together with the spectral intensity of the 100-fs laser pulse used in our model (the pulse is shown in the inset). The grey dashed lines highlight the different vibronic transitions, demonstrating that only the 0–2 transition is resonant with the laser pulse employed in the present model. **C**: The normalized absorption spectra for the three excited states considered in the OH model are depicted together with the spectral intensity of the 1-fs laser pulse used in our model (the pulse is shown in the inset). The pulse spectral intensity targets all three excited states.

As stated above, our model features four diabatic electronic states: the bound $X^2\Pi$ and $A^2\Sigma^+$ states along with the dissociative $1^2\Sigma^-$ and $1^2\Delta$ states (see Fig. 1A). Following Korolkov and Paramonov, we ignore the double degeneracy of both $X^2\Pi$ and $1^2\Delta$ states. The diabatic potential energy curves are represented with an extended Rydberg function,

$$V_i(R) = -D_i [1 + a_i(R - R_i) + b_i(R - R_i)^2 + c_i(R - R_i)^3] \exp[-\gamma_i(R - R_i)] + D_i^0. \quad (18)$$

The parameters for the diabatic potential energy curves of the $X^2\Pi$ and $A^2\Sigma^+$ states were reproduced from Korolkov and Paramonov,²⁹ while those for the potential energy curves of the $1^2\Sigma^-$ and $1^2\Delta$ states were fitted to electronic energies obtained with RMS-SA6-CASPT2(7e,5o) combined with a cc-pVTZ basis for O and cc-pVDZ for H, performed in OpenMolcas v22.06,³⁰ see Tab. 1. The diabatic couplings are set to zero between all electronic states following Korolkov and Paramonov²⁹ and further confirmed by our RMS-CASPT2 calculations. Hence, the adiabatic potential energy curves have the same shape as the diabatic ones; they are just reordered such that the adiabatic potential energy curves never cross. The adiabatic states are labelled D_1 – D_4 , highlighting the doublet spin multiplicity.

Table 1: Parameters of the extended Rydberg function [Eq. (18)] for the potential energy curves and the transition dipole moment (μ) in the diabatic basis. Parameters for the $X^2\Pi$ and $A^2\Sigma^+$ states were reproduced from Ref. 29, only with a shift of the D^0 parameter by 75.49253 a.u. such that the first dissociation limit is at zero energy.

Parameter	$V_{X^2\Pi}$	$V_{A^2\Sigma^+}$	$V_{1^2\Sigma^-}$	$V_{1^2\Delta}$	μ
a (a.u. ⁻¹)	2.44875	3.02658	0.66099	0.72427	1.07015
b (a.u. ⁻²)	1.60999	2.69337	1.35253	0.88319	0.21032
c (a.u. ⁻³)	0.69090	1.12086	$-1.19901 \cdot 10^{-5}$	-0.21862	-0.83399
γ (a.u. ⁻¹)	2.48159	3.06578	2.31260	2.24620	1.60275
D (a.u.)	0.16905	0.09297	-0.24267	-0.17649	-0.28015
D^0 (a.u.)	0.00000	0.07294	0.00000	0.07294	0.00334
R (a.u.)	1.84000	1.92000	1.54517	1.71368	0.98682

In the following, we will focus on the interaction between the OH radical and two different laser pulses. The laser pulse interacts with the molecule through the dipole approximation: $-\hat{\vec{\mu}}(\mathbf{r}, R) \cdot \vec{E}_0 E(t)$ where $\vec{\mu}(\mathbf{r}, R)$ is the dipole moment operator, \vec{E}_0 is the polarization of the electric field, and $E(t)$ is the time-dependent magnitude of electric field. The response of the molecule to the electric field is governed by the dipole matrix elements $\vec{\mu}_{IJ}(R) = \langle \Phi_I^{(\text{dia})}(R) | \hat{\vec{\mu}} | \Phi_J^{(\text{dia})}(R) \rangle_r$, i.e., the dipole moments (diagonal elements) and transition dipole moments (off-diagonal elements). The interaction strength then depends on the projection of the (transition) dipole moments onto the polarization vector, i.e., $\vec{\mu}_{IJ}(R) \cdot \vec{E}_0$. In the case of

the OH radical, all dipole moments are aligned with the molecular axis and thus perpendicular to all the transition dipole moments (which are perpendicular to the molecular axis) – see the inset in Fig. 1A. Thus, by defining the polarization of the laser pulse to be perpendicular to the molecular axis, the projection of the dipole moments onto the polarization vector of the pulse is zero, $\vec{\mu}_{II}(R) \cdot \vec{E}_0 = 0$, and the transition dipole moments are fully aligned with it, $\vec{\mu}_{IJ}(R) \cdot \vec{E}_0 = \mu_{IJ}(R)$. While this choice of alignment assumes preoriented molecules, e.g., by a strong IR field, it prevents vibrational transitions within a given electronic state and allows for purely electronic transitions (yet possibly with a vibrational component coupled with the electronic transition, as we shall see later). Finally, we note that our *ab initio* calculation shows that all transition dipole moments from the ground state have a similar direction and magnitude, while the transition dipole moments between excited states are negligible. Hence, we simplify the model by neglecting all transition dipole moments between excited states and set all the transition dipole moments from the ground electronic state to the same function:

$$\vec{\mu}_{X^2\Pi,J}(R) \cdot \vec{E}_0 = \mu(R), \quad \forall J. \quad (19)$$

The transition dipole moment $\mu(R)$ was also fitted to the extended Rydberg function using the data from Korolkov and Paramonov;²⁹ the fitting parameters are presented in Tab. 1.

Bringing together all the aforementioned elements, we obtain the final diabatic electronic Hamiltonian for our four-state model of the OH radical under the influence of an aligned laser pulse,

$$\mathbb{H}^{(\text{dia})} = \begin{pmatrix} V_{X^2\Pi} & 0 & 0 & 0 \\ 0 & V_{A^2\Sigma^+} & 0 & 0 \\ 0 & 0 & V_{1^2\Sigma^-} & 0 \\ 0 & 0 & 0 & V_{1^2\Delta} \end{pmatrix} - \begin{pmatrix} 0 & \mu & \mu & \mu \\ \mu & 0 & 0 & 0 \\ \mu & 0 & 0 & 0 \\ \mu & 0 & 0 & 0 \end{pmatrix} E(t), \quad (20)$$

which is used for the quantum dynamics simulations described in Section 3.3. The diabatic wave functions and potential energy curves are transformed to the adiabatic picture by diag-

onalization of $\mathbb{H}^{(\text{dia})}$. From now on, we will prioritize the adiabatic basis in our discussion and use the adiabatic states labels D_1 – D_4 .

3.2 100-fs and 1-fs laser pulses

The laser pulses employed in this work have the form of cosine oscillations modulated with a square sine envelope,

$$\vec{E}(t) = E_0 \sin^2\left(\frac{\pi t}{T}\right) \cos(\omega(t - T/2)) \quad \text{for } t \in [0, T], \quad (21)$$

where E_0 is the strength of the interaction, T is the duration period of the pulse, and ω is the frequency of the electric field oscillations.²⁹ Although laser pulses defined via the electric field \vec{E} instead of a vector potential are not generally in line with Maxwell’s equations, especially for short laser pulses, we carefully checked that our pulses do not violate Maxwell’s equations, following Ref. 31 and SI of Ref. 32.

We applied two different laser pulses in our work: a 100-fs pulse and a 1-fs pulse. The 100-fs pulse was motivated by Korolkov and Paramonov, who tuned such pulses to achieve 100% population transfers from the ground state (D_1) to selected vibrational states of the first excited electronic state D_2 . In this work, we reoptimized the pulse parameters to trigger a full population transfer to the third (second excited) vibrational state in the D_2 electronic state by keeping the duration of the pulse but varying the intensity E_0 and frequency ω . Our tuned laser pulse parameters are $T = 100$ fs, $E_0 = 0.0704$ a.u., and $\omega = 0.17365$ a.u. = 4.7253 eV. The pulse and its spectral intensity are depicted in Fig. 1B together with the normalized absorption spectrum of the D_2 ($A^2\Sigma^+$) state. Note that the pulse spectrum is in resonance solely with the corresponding $|D_1, \nu = 0\rangle \rightarrow |D_2, \nu = 2\rangle$ vibronic transition, and that the other vibronic transitions are far from resonance.

The second pulse we chose has a duration of 1-fs and mimics a typical pulse used in the

context of attochemistry. The parameters of this laser pulse are $T = 1$ fs, $E_0 = 0.5$ a.u., and $\omega = 0.55310$ a.u. = 15.051 eV. The pulse and its spectral intensity are depicted in Fig. 1C together with the normalized absorption spectrum of all the excited states. This ultrashort pulse targets all three excited states due to a sufficiently broad spectrum, and a coherent superposition of excited electronic states—an electronic wave packet—is expected to be formed as a result of the pulse, typical of attochemistry experiments.

3.3 Quantum dynamics of laser-excited OH in the BH and EF representations

The quantum dynamics of the OH radical under the influence of the 100-fs and 1-fs laser pulses were carried out in the BH representation using a diabatic basis with our in-house code QDyn v1.0.³³ The nuclear propagation employed a split-operator technique using the Fourier method for evaluating the kinetic energy operator. The time step was set to 0.1 a.t.u.²⁹ The distance R between the atoms of the OH molecule ranged from 0.5 to 8.0 a.u. and was discretised into 2048 grid points. Convergence with respect to both the time step and the grid size was verified. The diabatic wave functions and potential energy curves were transformed to the adiabatic basis by diagonalizing the diabatic Hamiltonian after propagation.

The EF quantities were not directly propagated using the EF equations of motion, as this is an unnecessarily labourious task. Instead, they were extracted from the diabatic BH wave functions.^{14,22,34,35} Note that obtaining EF quantities from the BH wave function is equivalent to their direct propagation, as there is a one-to-one transformation between BH expansion and EF.³⁶ This approach serves the purpose of demonstrating the two perspectives of photoexcitation since we are not interested in the EF propagation itself but rather in the behavior of the quantities unique to the EF formalism. The EF quantities were obtained under a gauge where the TDVP is set to zero, i.e., $A(R) = 0$. Results with a gauge, where the nuclear phase is set to zero, are provided in the Supporting Information. The EF quantities

were directly obtained from the QDyn v1.0 code.³³

Furthermore, we performed quantum dynamics simulations in the BH representation using a truncated basis (Hilbert space), i.e., by expanding the full molecular wave function as a linear combination of only selected vibronic states:

$$\Psi(\mathbf{r}, R; t) = \sum_{K=1}^{N_{\text{el}}} \sum_{v=0}^{N_{\text{vib}}} c_{K,v}(t) \chi_{K,v}(R) \Phi_K(\mathbf{r}; R), \quad (22)$$

where $\chi_{K,v}(R)$ is the v^{th} vibrational eigenstate of K^{th} electronic state $\Phi_K(\mathbf{r}; R)$, and $c_{K,v}(t)$ are the time-dependent expansion coefficients of the vibronic states $\chi_{K,v}(R) \Phi_K(\mathbf{r}; R)$. In this setup, only the expansion coefficients are time-dependent and propagated in the dynamics. The purpose of these calculations was to inspect the role of specific vibronic states in the dynamics of OH and assess the effect of basis set truncation on the outcomes of simulations. The vibrational eigenfunctions were obtained by imaginary-time quantum dynamics, as implemented in QDyn.³³ The Hamiltonian matrix elements between the vibronic states are provided in the Supporting Information. The quantum dynamics with a truncated basis were carried out with a 0.1 a.t.u. time step in the cQDyn v1.0 code.³⁷

4 Results and Discussion

We begin our analysis with the formation of a stationary molecular state upon photoexcitation with a 100-fs laser pulse. The BH and EF pictures of photoexcitation are contrasted, which allows us to offer a different interpretation of a stationary state photoexcitation than the one offered in monographs and textbooks. Follows a deeper investigation of the BH picture and the effect of basis set truncation, discussing the standard textbook concepts of resonance condition and vertical excitation. We then discuss the impact of a short, 1-fs laser pulse on the excited molecular state and the nuclear dynamics driven by a coherent superposition of excited electronic states.

4.1 Photoexcitation to a stationary molecular state

Let us start by discussing the photoexcitation of OH by the 100-fs laser pulse described in Sec. 3.2. The laser pulse has a very narrow spectral intensity targeting a single vibronic eigenstate of the hydroxyl radical (see Fig. 1B), resulting in the formation of a stationary molecular state (not a wave packet) after the pulse interaction ceases. Thus, the only dynamics triggered by this laser pulse should take place during the photoexcitation process, connecting the initial and final stationary states. The expected steps of this process are: OH in its stationary ground electronic and vibrational state (<0 fs) \rightarrow coupled electron-nuclear dynamics during the pulse interaction (0–100 fs) \rightarrow OH in a stationary vibrational state in the first excited electronic state (>100 fs). As such, the dynamics can be attributed purely to the formation of the excited molecular state, which is central to this paper.

We now investigate the photoexcitation mechanism from the BH and EF perspectives, focusing on the dynamics during the laser pulse connecting the two molecular stationary states. Snapshots of the dynamics in both representations are presented in Fig. 2 (an animation of the process is available using the following [link](#) for full inspection³⁸).

We shall start with the BH picture as it constitutes the typical representation of a photoexcitation taught to chemists (top row of Fig. 2). The 100-fs laser pulse fully depopulates the initial stationary molecular state (ground electronic and vibrational state $|D_1, \nu = 0\rangle$), transferring the whole population to the third vibrational state of the first excited electronic state ($|D_2, \nu = 2\rangle$). The final state remains stationary after the end of the pulse (>100 fs). The exclusive formation of the $|D_2, \nu = 2\rangle$ molecular state strictly obeys the resonance condition, as the laser pulse spectrum overlaps only with the $|D_1, \nu = 0\rangle \rightarrow |D_2, \nu = 2\rangle$ transition (see Fig. 1B). During the photoexcitation, the molecular process appears simple: the ground molecular state gradually depopulates while the $|D_2, \nu = 2\rangle$ state gains population. The BH nuclear densities for the two electronic states considered here ($|\chi_1|^2$ and $|\chi_2|^2$) do not exhibit any apparent dynamics except for gaining/losing amplitude (top row

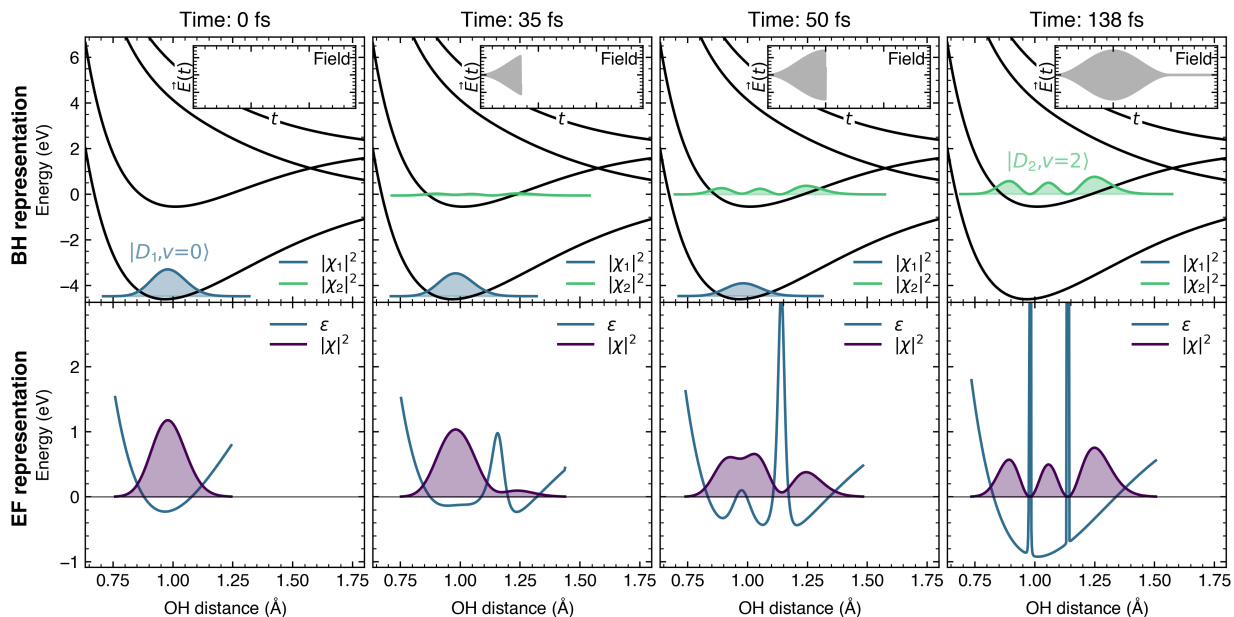


Figure 2: Snapshots of the OH photoexcitation with the 100-fs laser pulse in the BH (top row) and EF (bottom row) representations at four different time snapshots: 0, 35, 50, and 138 fs. The initial molecular state before the laser pulse interaction is observed at time 0 fs (first column), the final stationary molecular state is observed for $t > 100$ fs – the snapshot at 138 fs (last column) in this figure. Top panel: the BH nuclear densities for the adiabatic states ($|\chi_i|^2$) and their corresponding adiabatic potential energy curves (black) are represented. Lower panel: the total nuclear density ($|\chi|^2$) and the TDPEs (ϵ) are depicted. The insets contain the electric-field component of the laser pulse [$\vec{E}(t)$] up to the given time of the snapshot. An animated version of the plot is available using the following [link](#).³⁸

of Fig. 2). Hence, the photoexcitation seems to be a simple transfer of nuclear amplitude between two vibrational eigenstates in different electronic states, featuring no or minimal dynamics: a picture commonly introduced in photochemistry textbooks to describe a stationary photoexcitation process.

Moving to the EF, we now scrutinize the same process through the lens of the total nuclear density $|\chi(\mathbf{R}; t)|^2$ and the TDPEs $\epsilon(\mathbf{R}, t)$ (bottom row of Fig. 2). The initial TDPEs matches the D_1 potential energy curve, and $|\chi|^2$ corresponds to the ground-state nuclear density. Once the laser pulse arrives, the TDPEs starts evolving and develops a new minimum around 1.25 Å, see the snapshot of 35 fs in Fig. 2. This new minimum, separated from the original minimum (at around 1 Å) by an energy barrier, draws the nuclear density

towards longer bond lengths. We can identify this process as a tunnelling process through TD PES, with the barrier height dictating the tunnelling rate. Recall that TD PES reflects the effect of the electrons on the nuclei and that we set the laser polarization such that the nuclei are not directly affected by the laser pulse. Hence, the electric field of the laser pulse drives only the electrons, which in turn drive the nuclei. After 50 fs of irradiation, at the maximum of the laser pulse, enough nuclear density has reached the new minimum around 1.25 Å, and the increasing barrier height starts effectively reducing the tunnelling and stabilizing localization at 1.25 Å. Moreover, a new minimum has emerged around 1.1 Å by that time, giving rise to another energy barrier which begins to further split the nuclear density.^c Once the laser pulse interaction is over, both TD PES and the nuclear density remain stationary. The TD PES mimics the D_2 potential energy curve with the exception of the two singularities which developed from the energy barriers. These singularities create the nodes in the nuclear density and effectively block any tunnelling. Note that quantitatively the same results are achieved in the gauge where the nuclear phase is equal to zero (gauge common in multidimensional molecular systems), suggesting the validity of the presented results across gauges, see Supporting Information.

Four clear and major observations emerge from comparing the BH and EF pictures of the photoexcitation presented above:

Observation 1: EF clearly distinguishes electronic and nuclear dynamics, as these are captured separately by $\Phi(\mathbf{r}; t, \mathbf{R})$ and $\chi(\mathbf{R}; t)$. Since the laser field interacts only with the electrons in the present case, the nuclear wave function is unaffected in the early stages of the photoexcitation and starts evolving only later in response to the excited electrons. Hence, EF helps us to easily identify that the laser field affects the nuclei only indirectly through their interaction with the electrons via the TD PES. In contrast, the BH nuclear amplitudes, $\chi_I(\mathbf{R}, t)$, encompass both nuclear and electronic dynamics, which makes it challenging to

^cWe recommend watching the animations as they better depict the development of the barrier than the snapshots presented here.

distinguish between the electronic and the nuclear contribution to the evolution. Since the nuclear amplitudes evolve in the electronic states and transfer between them, a more detailed analysis is necessary to separate electronic and nuclear contributions and draw the conclusions above.

Observation 2: Both representations use different concepts to capture the photoexcitation: the BH representation features amplitude transfer between electronic states, while the EF representation employs barriers on the TD PES and tunnelling through them to capture the same effects.

Observation 3: The final nuclear density ($|\chi|^2$ in EF and $|\chi_2|^2$ in BH) has two nodes irrespective of the representation; however, these nodes have a different origin. While the nodes in the BH representation come naturally from the orthogonality of bound vibrational eigenfunctions,^{39,40} the nodes in the EF representation are enforced by the singularities in the TD PES. This observation is, however, not directly related to the photoexcitation process *per se*.^d

Observation 4: While EF highlights the rich nuclear dynamics through the total nuclear density and the electronic dynamics through TD PES during the photoexcitation process, the BH representation presents a seemingly minimal dynamics. In plain terms, both TD PES and the total nuclear density visibly evolve during the dynamics: TD PES creating new minima and developing barriers, the nuclear density tunnelling through these barriers and occupying the minima. Contrarily, the laser pulse in the BH representation simply depopulates the ground state and populates the final state without any apparent dynamics.

^dThe appearance of nodes in the nuclear wave function is not in disagreement with the extensive literature devoted to nodeless vibrational wave functions in the context of EF, as for instance Refs. 41–44. Specifically, when applying EF to stationary molecular eigenstates, the nuclear time-dependent Schrödinger equation (13) is replaced by a stationary Schrödinger equation featuring the exact potential energy surface – and the exact vector potential in more than one dimension. The lowest energy solution, yielding a nodeless wave function in the absence of symmetries, provides the vibrational component of the EF.^{43,44} While nodeless, such wave functions are reminiscent of the result shown in Fig. 2 at 138 fs since they are associated with ‘spiky’, yet non-singular, exact potential energy surfaces. By contrast, when the BOA limit is approached, the spiky potential develops singularities⁴⁴ as is the case at the end of the photoexcitation process with the 100-fs laser pulse.

The Observations above highlight the conceptual difference between the BH and EF representations and opportunities stemming from a change of perspective. Ensuing the last point, the following question arises: Where are the dynamics hidden in the BH representation? Since both EF and BH are equivalent representations of the same molecular wave function, the same amount of dynamics must also be encoded in the BH nuclear amplitudes. Guided by the dynamics observed within the EF representation, we propose now to further analyze the BH quantities, attempting to extract the seemingly missing dynamical picture and disentangle the nuclear and electronic contributions to the dynamics.

4.1.1 A different interpretation of photoexcitation in the Born–Huang picture

First, let us recall that the pulse spectral intensity effectively encompasses only the transition to the $|D_2, \nu = 2\rangle$ state; all other states lie far off resonance with the laser pulse employed. In particular, the spectral intensity for the excitation to $|D_1, \nu = 0\rangle$ is only 0.000007% of that to $|D_2, \nu = 2\rangle$. Following first order time-dependent perturbation theory—the common textbook approach to linear spectroscopy with long or continuous pulses—and the ensuing resonance condition, the molecular wave function can be expanded only in the basis of these two resonant vibronic states, $\chi_{D_1, \nu=0}(R) \Phi_{D_1}(\mathbf{r}; R)$ and $\chi_{D_2, \nu=2}(R) \Phi_{D_2}(\mathbf{r}; R)$, where $\chi_{D_1, \nu=0}(R)$ and $\chi_{D_2, \nu=2}(R)$ are the nuclear eigenfunctions for $\nu = 0$ and $\nu = 2$ in their respective electronic state. This resonance-based argument is central to standard spectroscopic reasoning and is consistent with the simulated dynamics in Fig. 2, which end in a pure $|D_2, \nu = 2\rangle$ state. Hence, if the two-state expansion were an adequate approximation, we would expect an essentially complete population transfer into $|D_2, \nu = 2\rangle$.

To test this two-state hypothesis, we can now expand the time-dependent molecular wave function in the basis of the two vibronic states described above (following Eq. (22)),

$$\Psi(\mathbf{r}, R; t) = c_1(t)\chi_{D_1, \nu=0}(R) \Phi_{D_1}(\mathbf{r}; R) + c_2(t)\chi_{D_2, \nu=2}(R) \Phi_{D_2}(\mathbf{r}; R). \quad (23)$$

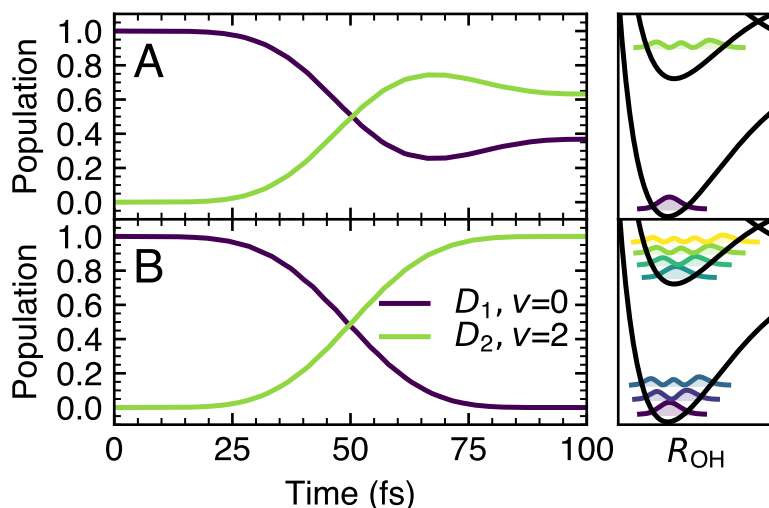


Figure 3: Populations of the $|D_1, v = 0\rangle$ (purple) and $|D_2, v = 2\rangle$ (green) states for simulations with a truncated expansion of the vibronic states: **A** two vibronic states, **B** seven vibronic states. The vibrational eigenstates used in the expansion are depicted in the right panels.

Before the laser pulse, the molecular wave function is described by $c_1(t) = 1$ and $c_2(t) = 0$, that is, a stationary OH molecule in its ground vibrational and electronic state. We can then propagate this approximate molecular wave function under the effect of the 100-fs laser pulse and depict the populations ($|c_1(t)|^2$ and $|c_2(t)|^2$) of the two resonant vibronic states, $|D_1, v = 0\rangle$ and $|D_2, v = 2\rangle$. The results of such a dynamics, depicted in Fig. 3A, show that this two-state picture is obviously invalid. This two-state approximation does not capture the full population transfer to the $|D_2, v = 2\rangle$ state, with the final population being only 0.63. Thus, the other off-resonant vibronic states must participate in the dynamics, although they are not apparent at first sight in Fig. 2. Extending our truncated expansion to the three lowest vibrational states of D_1 and four lowest vibrational states of D_2 is capable of capturing the full population transfer (Fig. 3B) in agreement with the full quantum-dynamics simulation presented above. Addition of any further vibronic states does not alter the resulting dynamics. This set of simulations highlights the dramatic role played by the neighboring vibronic states in the description of a stationary photoexcitation, even though they are off-

resonant. Simulations with various other combinations of vibronic states in the expansion are provided in the Supporting Information.

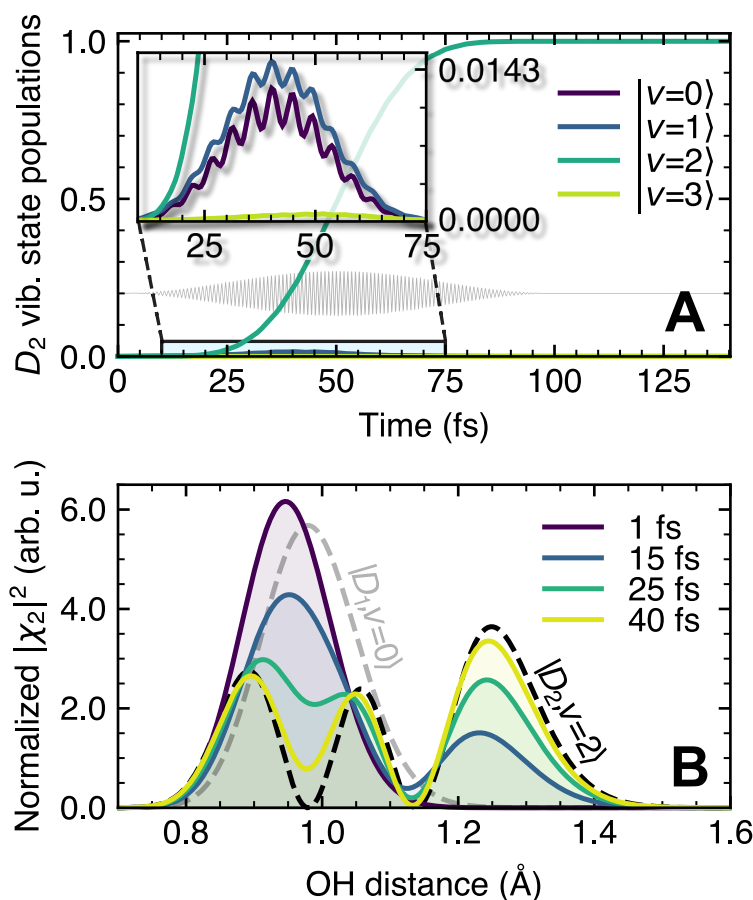


Figure 4: **A**: Populations of the vibrational states belonging to electronic state D_2 during the photoexcitation process. The legend uses a simplified notation where $|D_2, v = n\rangle$ is denoted as $|v = n\rangle$. The inset focuses on the off-resonant vibrational states between 10 and 75 fs. **B**: Normalized (time-dependent) nuclear density on D_2 ($|\chi_2|^2/\langle\chi_2|\chi_2\rangle$) for selected times of 1, 15, 25, and 40 fs. The dashed lines depict the normalized (stationary) nuclear densities of the initial $|D_1, v = 0\rangle$ state (grey) and final $|D_2, v = 2\rangle$ state (black).

To understand the impact of neighbouring vibronic states in the photoexcitation dynamics, let us return to the original quantum dynamics simulation in the BH representation (Fig. 2A) and decompose the D_2 nuclear amplitude $\chi_2(R; t)$ into the vibrational eigenfunctions for this electronic state, see Fig. 4A. The second vibrational state, $|D_2, v = 2\rangle$, dominates the decomposition; the remaining vibrational states are barely visible in the graph using a full scale. The maximum population between the off-resonant state reaches $|D_2, v = 1\rangle$,

peaking to 1.5% at 40 fs, closely followed by the population of $|D_2, \nu = 0\rangle$. A non-negligible population is also acquired by the $|D_2, \nu = 3\rangle$ state. Despite such low populations, these intermediate vibrational states make up for the large discrepancy observed in Fig. 3 and act as mediators for the full population transfer, compared to a final population of only 63% if these vibronic states are omitted.

While the crucial role of the off-resonant states may seem somewhat surprising from the perspective of the resonance condition, their necessity becomes clearer by focusing on the excited-state density $|\chi_2|^2$, see Fig. 4B. Note that the initial $|D_1, \nu = 0\rangle$ state and the final $|D_2, \nu = 2\rangle$ state densities do not fully overlap in configuration space: the maximum of the $|D_2, \nu = 2\rangle$ state density lies in a region around 1.25 Å where the initial $|D_1, \nu = 0\rangle$ density decays effectively to zero. Since nuclei cannot “jump” through space, the nuclear density must flow smoothly and seamlessly to connect the initial and final density, as clearly depicted by the EF simulations in Fig. 2. The normalized nuclear density in D_2 at 1 fs (dark purple curve in Fig. 4B), i.e., right after the pulse is initiated, resembles the initial nuclear density for $|D_1, \nu = 0\rangle$ (dashed grey curve in Fig. 4B); the shift to shorter bond lengths is a consequence of the linear transition dipole moment. We note that describing the excited nuclear wave function following photoexcitation as the ground-state nuclear wave function multiplied by the (position-dependent) transition dipole moment is known as the ‘sudden/vertical approximation’ in physical and theoretical chemistry.¹⁷ As time progresses, the nuclear density in D_2 gradually evolves towards longer bond lengths and populates the region around 1.25 Å, also forming a node at 0.98 Å. The off-resonant vibrational states are necessary to facilitate this smooth flow of nuclear density, and their population increases as seen in the inset of Fig. 4A. At 40 fs, the nuclear density in D_2 (yellow curve in Fig. 4B) almost reaches the shape of the final $|D_2, \nu = 2\rangle$ state (dashed black curve in Fig. 4B). Thus, the off-resonant vibrational states are no longer necessary to accommodate the nuclear density, and their populations decline. The off-resonant vibrational states are, therefore, indispensable interme-

diates facilitating a smooth transfer of nuclear density from the sudden/vertical excitation to the nuclear density of the final state. Without the off-resonant vibrational states, the nuclear density would be forced to suddenly jump in configuration space.^e

The concept of sudden excitation This detailed analysis of a stationary photoexcitation reveals how the coupled electron-nuclear dynamics during the photoexcitation is encoded in the BH representation. The discrete set of electronic states gives rise to the concept of sudden/vertical excitation, which reflects the fast initial response of the electrons to the laser field compared to the slower nuclear response. As such, the sudden excitation prompts us to picture photoexcitation as a vertical promotion of nuclei to a higher electronic state. The vertically promoted nuclear density then evolves on the given electronic potential to form the final state, connecting this final state smoothly to the initial state. The concept of sudden excitation becomes redundant once we focus on the total nuclear density, a quantity inherent to the EF representation. The total nuclear density must evolve smoothly and cannot suddenly change its position, as seen in the EF simulation. The initial response of the molecule to the electric field at the very beginning of the laser pulse is purely electronic, and the EF ansatz fully captures this in the time-dependent electronic wave function. The nuclei are impacted only later by responding to the electrons. Hence, the whole process can be understood without any vertical excitation, which belongs solely to the BH expansion, and without the use of a set of electronic states. Based on these arguments, we argue that the EF representation is perhaps more suited to decipher the fundamental process inherent to photoexcitation dynamics.

On the resonance condition Finally, we briefly comment on the concept of the resonance condition. The pulse spectral intensity (square of the pulse energy spectrum) reflects the

^eNote that for the two-state approximate model in Fig. 3A, the nuclear density in D_2 depicted in Fig. 4B would align with the black dashed line of $|D_2, \nu = 2\rangle$ throughout the whole simulation.

energy composition of the complete laser pulse, i.e., of the pulse over its entire duration. Therefore, the resonance condition based on the pulse spectral intensity allows us to infer the final molecular state after the photoexcitation. Since our pulse spectral intensity encompasses solely the transition to the $|D_2, \nu = 2\rangle$ state, only the resonant $|D_1, \nu = 0\rangle$ and $|D_2, \nu = 2\rangle$ states should be populated after the laser pulse interaction is over, which is consistent with our quantum dynamics simulations. However, the resonance condition based on the pulse spectral intensity does not apply for dynamics during the photoexcitation, as demonstrated in Fig. 3A. At the beginning of the laser pulse, the corresponding (transient) spectral intensity would be much wider in energy due to the time-energy uncertainty principle, targeting a broader range of transitions.^f As the pulse progresses, the energy spectrum narrows, these transitions are getting out of resonance, and populations of the corresponding states are decreasing. As a thought experiment, abruptly (and artificially) stopping our laser pulse after its maximum at 50 fs would mean that all the neighbouring vibrational states depicted in Fig. 3B are in resonance with the initial state.^g Therefore, considerations based on the pulse spectral intensity and resonance condition are valid for the molecular states of the system after photoexcitation, but cannot be relied on for describing dynamics during photoexcitation.

4.2 Photoexcitation to a coherent superposition of electronic states

In this Section, our attention will be focused on ultrashort, few-cycle laser pulses: the cornerstone of attochemistry. Such ultrashort pulses typically create a molecular state in a coherent superposition of electronically excited states; in the present case, the 1-fs pulse targets all the excited electronic states D_2 to D_4 of OH (see the spectral intensity in Fig. 1C). Photoexcitation with this 1-fs pulse will, therefore, also promote OH in its dissociative electronic

^fThe short-time duration and wide energy spectrum justify the vertical excitation concept observed at the beginning of our dynamics.

^gWe note that our discussion follows the populations of the off-resonant vibrational states of D_1 and D_2 , completely omitting the off-resonant *electronic* states D_3 and D_4 . By the same mechanism, these off-resonant electronic states were also populated; however, they landed only 0.06% population at their peak—a negligible number compared to 1.5% of the vibrational $|D_2, \nu = 1\rangle$ state.

states, unlike the 100-fs pulse. Hence, this ultrashort pulse allows us to investigate how attochemistry emerges from the BH and the EF representations.

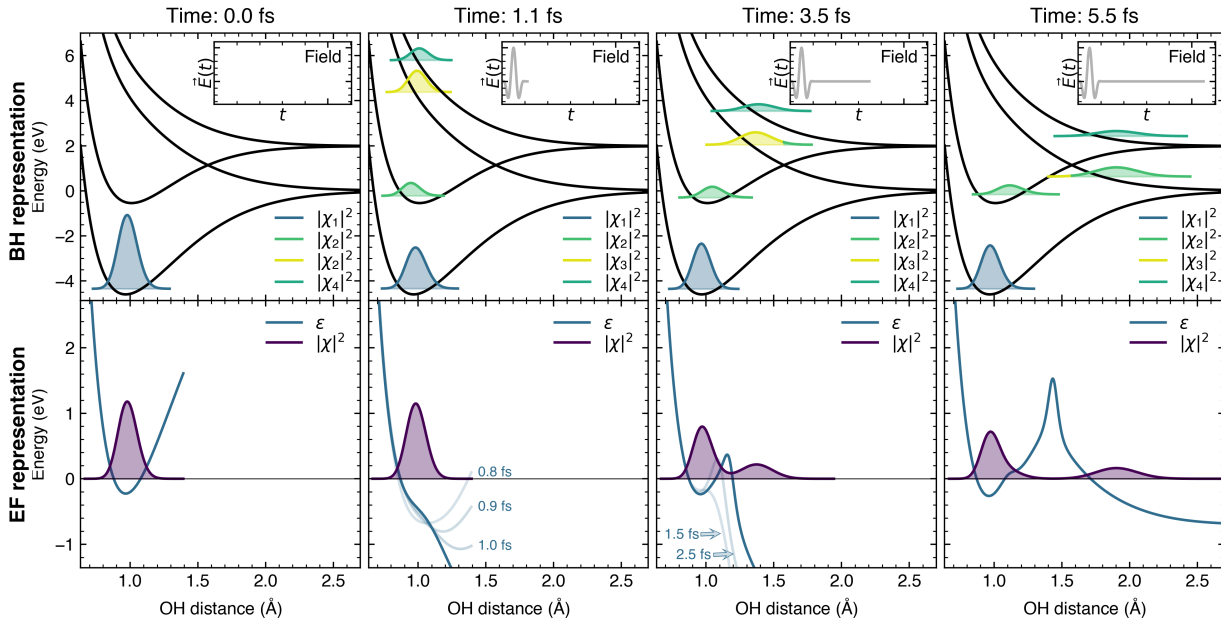


Figure 5: Snapshots of the photoexcitation of OH with a 1-fs laser pulse in the BH (top panel) and the EF (bottom panel) representations at four times: 0, 1.1, 3.5, and 5.5 fs. For the BH representation, we plot the BH nuclear densities for the adiabatic states ($|\chi_i|^2$) and their corresponding adiabatic potential energy curves (black). For the EF representation, we plot the total nuclear density ($|\chi|^2$) and the TDPE (ϵ). The transparent lines in the lower panel depict TDPEs at other snapshot times. The insets contain the laser pulse electric field $\vec{E}(t)$ up to the given time of the snapshot. Animated version of the plot is available using the following [link](#).³⁸

We begin the discussion with the BH representation again (upper panel of Fig. 5). The laser pulse leads to a nearly equal coherent population of all three excited electronic states, without any visible dynamics during the photoexcitation process apart from the nuclear amplitude transfer (see the animated plot available using the following [link](#)).³⁸ The excited-state densities right after the pulse (1.1 fs in the upper panel of Fig. 5) resemble the ground-state nuclear density in both shape and position, in line with the concept of sudden/vertical excitation discussed in the previous Section. As time progresses, the nuclear densities in D_3 and D_4 follow their respective dissociative electronic curves, while the nuclear densities in D_1

and D_2 remain in the bound regions of their electronic potentials. Between 3.5 and 5.5 fs, the dissociating nuclear wave packet in D_3 passes the D_3/D_2 crossing point and transfers amplitude to the lower electronic state (D_2).

Let us now move to the EF representation for the very same photoexcitation process (bottom panel of Fig. 5). During the laser pulse, the originally bound TD PES (mimicking the bound D_1 electronic curve) experiences two separate dynamics: (i) it oscillates up and down following the electric field of the pulse without changing its shape, and (ii) it gets shallow towards larger bond distances near the end of the pulse (after around 0.8 fs), eventually opening the dissociation channel. Both motions are better seen in the animated version of the plot available using the following [link](#).³⁸ Once the laser pulse is over, the path to dissociation created by the TD PES is fully open and without any barriers, and the nuclear density evolves towards larger OH bond distances: the molecule starts dissociating. At 3.5 fs, the nuclear density is almost split into two parts, now separated by a small barrier in TD PES. At 5.5 fs, the two densities are completely separated, evolving on their corresponding parts of TD PES. These two separate minima of the TD PES are connected by a large barrier, causing the complete disconnection of the two nuclear densities.

Contrary to the long 100-fs pulse, the ultrashort 1-fs laser pulse does not trigger any significant nuclear dynamics during the photoexcitation; only the electrons respond within this time scale. How is this pulse scenario portrayed in the two representations? In the BH representation, this purely electronic response appears as a vertical promotion of nuclear amplitudes. The actual nuclear dynamics only set in after the pulse, when the nuclear amplitudes begin to evolve on the corresponding potential energy surface of their electronic state. Yet the nuclear dynamics might be cumbersome to infer from the nuclear amplitudes since the electronic dynamics intertwine with them.

The EF representation appears more transparent once again to disentangle nuclear motion resulting from a photoexcitation with an ultrashort pulse. The total nuclear density remains

unchanged during the pulse, fully reflecting the absence of nuclear response to the ultrashort laser pulse. The nuclear dynamics begin just at the end of the pulse, when the nuclei start feeling the driving force created by the excited electrons leading to a partial dissociation. Hence, the EF representation offers a clear picture of the nuclear motion and how it is influenced by the electronic dynamics, manifested in TDPEs.

5 Conclusions

In this work, we examined the photoexcitation process of a molecule, OH radical, using two different representations of the molecular wave function: the Born–Huang (BH) expansion and the exact factorization (EF), comparing their conceptual implications. We find that the EF representation is more intuitive for understanding the formation of an excited molecular state upon photoexcitation: EF clearly distinguishes nuclear and electronic response to the laser field during photoexcitation. In contrast, the BH representation intertwines both electronic and nuclear responses to the field within the nuclear amplitudes, complicating their separate analysis. Hence, EF constitutes a suitable representation for depicting photoexcitation and possibly even modelling.

The four-state model of the OH molecule developed for this work allowed us to explore two distinct photoexcitation scenarios: irradiation of the molecule by a long pulse and an ultrashort pulse. In the long-pulse scenario, a 100-fs pulse targets a single excited vibronic state, forming a *stationary* final molecular state. The dynamics connecting the initial and final stationary molecular states can be thus attributed purely to the photoexcitation process. Both representations depict this photoexcitation scenario using different concepts: the BH representation relies on the amplitude transfer between electronic states, while EF employs barriers on TDPEs and tunnelling to steer the nuclear dynamics triggered by the photoexcitation process. The picture of photoexcitation with tunnelling offers a novel perspective on

photoexcitation dynamics beyond BH amplitude transfer between electronic states.

EF offered a somewhat clearer conceptual picture for investigating nuclear dynamics during photoexcitation: while EF uses one compact nuclear density for all nuclei, the BH representation creates a notion of separate bundles of nuclei distributed among the electronic states. In the present case, the EF nuclear density clearly depicts the nuclear motion by smoothly evolving between the initial and final states, guided by the TD PES. On the contrary, the two BH (adiabatic) nuclear amplitudes involved appear seemingly stationary, only transferring population between the resonant vibronic states. Uncovering the nuclear dynamics—clearly observed in EF—requires a closer investigation of the two nuclear amplitudes. The well-known concept of vertical excitation emerges from such an investigation, indicating that the initial nuclear amplitude promoted to the excited state is a projection of the ground-state amplitude. However, the vertical excitation concept only demonstrates that nuclei remain stationary during the excitation of electrons, and is redundant in the EF framework.

Furthermore, we touched upon the concept of the resonance condition and its use in photodynamics. The resonance condition dictates what states are populated after the laser pulse interaction, making it a useful tool for selecting initial states for the subsequent excited-state dynamics without modelling the photoexcitation explicitly. Excluding the off-resonant states in such cases is a common practice. However, we demonstrated that the off-resonant states are essential during photoexcitation: they facilitate the formation of the final resonant states, albeit they disappear once the interaction ceases. The neglect of off-resonant states can make a crucial impact on the final state formed by the pulse. Insufficient basis of (off-resonant) states in methods for explicit modelling of photoexcitation, such as XFAIMS⁴⁵ or EOE,⁴⁶ can have a quality-determining impact on the results.

In the ultrashort (attochemical) pulse regime, only the light electrons manage to respond to the few-cycle pulse. The BH representation depicts this event as a vertical excitation of nuclear amplitudes, creating a coherent superposition of electronic states—an electronic wave

packet. The following evolution of nuclear amplitudes then captures both the dissociation of nuclei and damping of the electronic coherences, again blending electronic and nuclear dynamics. In the EF picture, the molecular response to the field is captured purely by the electronic wave function. The nuclear density remains untouched during the pulse and starts evolving only later in response to the excited electrons (via TD PES). Hence, EF allows to separate the fast electronic dynamics driven by attosecond pulses from the following nuclear dynamics driven by the excited electronic wave packet.

This separation can be advantageous for practical attochemical simulations, often relying on static nuclei or mean-field Ehrenfest trajectories.^{47–50} Both approaches benefit from the techniques of time-dependent quantum chemistry for propagating the electronic dynamics coupled to laser pulses, incompatible with standard methods for nonadiabatic dynamics based on the BH expansion. However, they suffer from the lack of decoherence due to nuclear motions,^{51,52} which damps the electronic coherence on a short femtosecond timescale.^{47,53} Presented results suggest that methods based on EF, such as CT-MQC,⁵⁴ present potential alternatives for simulating attochemistry. CT-MQC possesses the same advantages as Ehrenfest dynamics, yet captures decoherence effects exactly.^{55,56} Note that recent efforts to apply trajectory surface hopping methods, the working class of femtochemistry, for simulations with coherent superposition of electronic states were shipwrecked on the cliffs of decoherence,^{51,52,57} highlighting the ongoing search for methodology suitable for attochemistry.⁴⁷

To summarize, our work highlights that the EF of the molecular wave function offers a superior conceptual tool than the BH representation for describing photoexcitation in molecules. EF benefits from the clear separation of nuclear and electronic response to the field and ensuing dynamics. This separation not only simplifies the analysis of nuclear dynamics during photoexcitation but also makes EF a promising framework for attochemistry simulations, e.g., with its trajectory-based CT-MQC method.

Acknowledgement

Jiří Janoš thanks Jiří Suchan for insightful discussions on photoexcitation and the resonance condition. This work was supported from the grant of Specific university research - grant No A2_FCHI_2025_053. This work was supported by the project "The Energy Conversion and Storage", funded as project No. CZ.02.01.01/00/22_008/0004617 by Programme Johannes Amos Comenius, call Excellent Research. BFEC acknowledges funding from EPSRC for the grants EP/V026690/1, EP/Y01930X/1, and EP/X026973/1.

Supporting Information Available

Supporting Information contains: details of fitting the OH radical model Hamiltonian, an extended set of quantum dynamics simulations with a truncated basis set, and a detailed decomposition of the EF quantities along the dynamics in different gauges. (PDF)

References

- (1) Von Grotthuss, T. Auszug aus vier Abhandlungen Physikalisch-chemischen Inhalts. Annalen der Physik **1819**, 61, 50–74.
- (2) Draper, J. W. XXX. On some analogies between the phænomena of the chemical rays, and those of radiant heat. The London, Edinburgh, and Dublin Philosophical Magazine and Journal of Science **1841**, 19, 195–210.
- (3) Persico, M.; Granucci, G. Photochemistry: A Modern Theoretical Perspective; Springer, 2018.
- (4) Suchan, J.; Hollas, D.; Curchod, B. F. E.; Slavíček, P. On the importance of initial conditions for excited-state dynamics. Faraday Discussions **2018**, 212, 307–330.

- (5) Janoš, J.; Slavíček, P.; Curchod, B. F. E. Selecting Initial Conditions for Trajectory-Based Nonadiabatic Simulations. Accounts of Chemical Research **2025**, 58, 261–270.
- (6) Michl, J.; Bonačić-Koutecký, V. Electronic Aspects of Organic Photochemistry; John Wiley and Sons, New York, 1990.
- (7) Turro, N. J.; Ramamurthy, V.; Scaiano, J. C. Principles of molecular photochemistry: an introduction; University Science Books, 2009.
- (8) Born, M.; Huang, K. Dynamical Theory of Crystal Lattices; Oxford University Press: Oxford, 1954.
- (9) Domcke, W., Yarkony, D., Köppel, H., Eds. Conical Intersections: Electronic Structure, Dynamics & Spectroscopy; World Scientific, 2004; Vol. 15.
- (10) Worth, G. A.; Cederbaum, L. S. Beyond Born-Oppenheimer: molecular dynamics through a conical intersection. Annual Review of Physical Chemistry **2004**, 55, 127–158.
- (11) Agostini, F.; Curchod, B. F. Different flavors of nonadiabatic molecular dynamics. WIREs Computational Molecular Science **2019**, 9, 1–21.
- (12) Abedi, A.; Maitra, N. T.; Gross, E. K. U. Exact Factorization of the Time-Dependent Electron-Nuclear Wave Function. Physical Review Letters **2010**, 105, 123002.
- (13) Abedi, A.; Maitra, N. T.; Gross, E. K. U. Correlated electron-nuclear dynamics: Exact factorization of the molecular wavefunction. The Journal of Chemical Physics **2012**, 137, 22A530.
- (14) Agostini, F.; Curchod, B. F. E. When the exact factorization meets conical intersections ... European Physical Journal B **2018**, 91, 141.
- (15) Born, M.; Oppenheimer, R. Zur Quantentheorie der Molekeln. Annalen der Physik **1927**, 389, 457–484.

- (16) Agostini, F.; Curchod, B. F. E. A pictorial (and hopefully pedagogical) discussion on the Born–Oppenheimer approximation. Foundations of Chemistry **2025**,
- (17) Prlj, A.; Taylor, J. T.; Janoš, J.; Lognon, E.; Hollas, D.; Slavíček, P.; Agostini, F.; Curchod, B. F. E. Best practices for nonadiabatic molecular dynamics simulations. Living Journal of Computational Molecular Science **2026**, *7*, 4157.
- (18) Baer, M. Beyond Born–Oppenheimer: Conical Intersections and Electronic Nonadiabatic Coupling Terms; Wiley, 2006.
- (19) Tully, J. C. Perspective: Nonadiabatic dynamics theory. Journal of Chemical Physics **2012**, *137*, 22A301.
- (20) Yarkony, D. R.; Xie, C.; Zhu, X.; Wang, Y.; Malbon, C. L.; Guo, H. Diabatic and adiabatic representations: Electronic structure caveats. Computational and Theoretical Chemistry **2019**, *1152*, 41–52.
- (21) Agostini, F.; Tavernelli, I.; Ciccotti, G. Nuclear quantum effects in electronic (non)adiabatic dynamics. The European Physical Journal B **2018**, *91*, 139.
- (22) Agostini, F.; Abedi, A.; Suzuki, Y.; Min, S. K.; Maitra, N. T.; Gross, E. K. The exact forces on classical nuclei in non-adiabatic charge transfer. Journal of Chemical Physics **2015**, *142*, 084303.
- (23) Ibele, L. M.; Pieroni, C.; Talotta, F.; Curchod, B. F.; Lauvergnat, D.; Agostini, F. Comprehensive Computational Chemistry; Elsevier, 2024; Vol. 4; pp 188–211.
- (24) Agostini, F.; Gross, E. K. U. Quantum Chemistry and Dynamics of Excited States; Wiley, 2020; pp 531–562.
- (25) Agostini, F.; Gross, E.; Curchod, B. F. E. Electron-nuclear entanglement in the time-

- dependent molecular wavefunction. Computational and Theoretical Chemistry **2019**, 1151, 99–106.
- (26) Tu, M. W.-Y.; Gross, E. K. U. Electronic decoherence along a single nuclear trajectory. Physical Review Research **2025**, 7, 043075.
- (27) Gossel, G. H.; Lacombe, L.; Maitra, N. T. On the numerical solution of the exact factorization equations. Journal of Chemical Physics **2019**, 150, 154112.
- (28) Stetzler, J.; Garashchuk, S.; Rassolov, V. Factorised electron-nuclear dynamics with effective complex potential: on-the-fly implementation for H_2^+ in a laser field. Molecular Physics **2026**, e2611404.
- (29) Korolkov, M. V.; Paramonov, G. K. Vibrationally state-selective electronic excitation of diatomic molecules by ultrashort laser pulses. Physical Review A - Atomic, Molecular, and Optical Physics **1998**, 57, 4998–5001.
- (30) Li Manni, G.; Fdez. Galván, I.; Alavi, A.; Aleotti, F.; Aquilante, F.; Autschbach, J.; Avagliano, D.; Baiardi, A.; Bao, J. J.; Battaglia, S. et al. The OpenMolcas Web: A Community-Driven Approach to Advancing Computational Chemistry. Journal of Chemical Theory and Computation **2023**, 19, 6933–6991.
- (31) Madsen, L. B. Gauge invariance in the interaction between atoms and few-cycle laser pulses. Physical Review A **2002**, 65, 053417.
- (32) Janoš, J.; Slavíček, P.; Curchod, B. F. E. Including Photoexcitation Explicitly in Trajectory-Based Nonadiabatic Dynamics at No Cost. The Journal of Physical Chemistry Letters **2024**, 15, 10614–10622.
- (33) Janoš, J.; Suchan, J.; Slavíček, P. QDyn: Quantum Dynamics code. 2025; <https://github.com/PHOTOX/qdyn>.

- (34) Ibele, L. M.; Curchod, B. F. E.; Agostini, F. A Photochemical Reaction in Different Theoretical Representations. The Journal of Physical Chemistry A **2022**, 126, 1263–1281.
- (35) Curchod, B. F. E.; Agostini, F.; Gross, E. K. U. An exact factorization perspective on quantum interferences in nonadiabatic dynamics. The Journal of Chemical Physics **2016**, 145, 034103.
- (36) Schürger, P.; Lassmann, Y.; Agostini, F.; Curchod, B. F. E. On the connection between the exact factorization and the Born–Huang representation of the molecular wavefunction. The Journal of Chemical Physics **2025**, 162.
- (37) Janoš, J. cQDyn: coefficient-based Quantum Dynamics. 2025; <https://github.com/JanosJiri/cqdyn>.
- (38) Janoš, J. Supplementary animations for "On the interpretation of molecular photoexcitation with long and ultrashort laser pulses". 2025; <https://github.com/JanosJiri/Photoexcitation-From-Different-Perspectives>.
- (39) Couran, R.; Hilbert, T. D. Methods of mathematical physics; Wiley Interscience, 1953.
- (40) Teschl, G. Mathematical methods in quantum mechanics: With applications to Schrödinger operators, 2nd ed.; Graduate Studies in Mathematics; American Mathematical Society: Providence, Rhode Island, 2014; Vol. 157; pp 250–256.
- (41) Hunter, G. Nodeless wave function quantum theory. International Journal of Quantum Chemistry **1980**, 9, 133.
- (42) Hunter, G. Nodeless wave functions and spiky potentials. International Journal of Quantum Chemistry **1981**, 19, 755–761.

- (43) Foster, P. W.; Peters, W. K.; Jonas, D. M. Nonadiabatic eigenfunctions can have conical nodes. Chemical Physics Letters **2017**, 683, 268–275.
- (44) Kocák, J.; Schild, A. Nodeless wave functions, spiky potentials, and the description of a quantum system in a quantum. Physical Review Research **2021**, 3, 033194.
- (45) Mignolet, B.; Curchod, B. F. E.; Martínez, T. J. Communication: XFAIMS–eXternal Field Ab Initio Multiple Spawning for electron-nuclear dynamics triggered by short laser pulses. The Journal of Chemical Physics **2016**, 145, 191104.
- (46) Grünewald, L.; van Dam, L.; Mai, S. An Excitation Strategy for the Initial Condition Generation for Surface Hopping Trajectories Using Electron-Only Dynamics Including Explicit Laser Pulses. Journal of Chemical Theory and Computation **2025**, 21, 12741–12754.
- (47) Calegari, F.; Martin, F. Open questions in attochemistry. Communications Chemistry **2023**, 6, 184.
- (48) Lara-Astiaso, M.; Ayuso, D.; Tavernelli, I.; Decleva, P.; Palacios, A.; Martín, F. Decoherence, control and attosecond probing of XUV-induced charge migration in biomolecules. A theoretical outlook. Faraday Discussions **2016**, 194, 41–59.
- (49) Lara-Astiaso, M.; Galli, M.; Trabattoni, A.; Palacios, A.; Ayuso, D.; Frassetto, F.; Poletto, L.; De Camillis, S.; Greenwood, J.; Decleva, P. et al. Attosecond Pump–Probe Spectroscopy of Charge Dynamics in Tryptophan. The Journal of Physical Chemistry Letters **2018**, 9, 4570–4577.
- (50) Palacios, A.; Martín, F. The quantum chemistry of attosecond molecular science. WIREs Computational Molecular Science **2020**, 10, e1430.
- (51) Mannouch, J. R.; Kelly, A. Toward a Correct Description of Initial Electronic Coherence

- in Nonadiabatic Dynamics Simulations. The Journal of Physical Chemistry Letters **2024**, 15, 11687–11695.
- (52) Tran, T.; Ferté, A.; Vacher, M. Simulating Attochemistry: Which Dynamics Method to Use? Journal of Physical Chemistry Letters **2024**, 15, 3646–3652.
- (53) Vacher, M.; Bearpark, M. J.; Robb, M. A.; Malhado, J. P. Electron Dynamics upon Ionization of Polyatomic Molecules: Coupling to Quantum Nuclear Motion and Decoherence. Physical Review Letters **2017**, 118, 083001.
- (54) Min, S. K.; Agostini, F.; Gross, E. K. U. Coupled-Trajectory Quantum-Classical Approach to Electronic Decoherence in Nonadiabatic Processes. Physical Review Letters **2015**, 115, 073001.
- (55) Curchod, B. F. E.; Agostini, F.; Tavernelli, I. CT-MQC – a coupled-trajectory mixed quantum/classical method including nonadiabatic quantum coherence effects. The European Physical Journal B **2018**, 91, 168.
- (56) Agostini, F.; Gross, E. K. U. Ultrafast dynamics with the exact factorization. The European Physical Journal B **2021**, 94, 179.
- (57) Villaseco Arribas, E.; Maitra, N. T.; Agostini, F. Nonadiabatic dynamics with classical trajectories: The problem of an initial coherent superposition of electronic states. Journal of Chemical Physics **2024**, 160, 054102.

TOC Graphic



Supporting Information:

**On the interpretation of molecular
photoexcitation with long and ultrashort laser
pulses**

Jiří Janoš,^{*,†,‡} Federica Agostini,[¶] Petr Slavíček,[†] and Basile F. E. Curchod^{*,‡}

[†]*Department of Physical Chemistry, University of Chemistry and Technology, Technická 5,
Prague 6, 166 28, Czech Republic*

[‡]*Centre for Computational Chemistry, School of Chemistry, University of Bristol, Bristol
BS8 1TS, United Kingdom*

[¶]*Sorbonne Université, CNRS, LCT UMR 7616, Paris 75005, France*

E-mail: jiri.janos@vscht.cz; basile.curchod@bristol.ac.uk

Contents

1	Fitting the potential energy curves and transition dipole moments to build a four-state model Hamiltonian for the OH radical	S-3
2	Quantum dynamics within a truncated basis of vibronic states	S-6
3	Decomposition of the TDPES into its gauge-dependent and gauge-independent components, and test of different gauges	S-7
3.1	100-fs pulse in the zero-vector-potential gauge	S-8
3.2	1-fs pulse in the zero-vector-potential gauge	S-9
3.3	100-fs pulse in the zero-nuclear-phase gauge	S-10
3.4	1-fs pulse in the zero-nuclear-phase gauge	S-11
	References	S-12

1 Fitting the potential energy curves and transition dipole moments to build a four-state model Hamiltonian for the OH radical

As stated in the main text, our model Hamiltonian for the hydroxyl radical is based on a Hamiltonian developed by Korolkov and Paramonov.^{S1} Their diabatic Hamiltonian consists of two electronic states— $X^2\Pi$ and $A^2\Sigma^+$ —which were fitted to extended Rydberg functions (see the main text for a definition). In this work, we extended this Hamiltonian by including two more electronic states: $1^2\Sigma^-$ and $1^2\Delta$. For that purpose, we calculated the potential energy curves (PECs) of the OH radical at the RMS-CASPT2 level of theory with a cc-pVTZ basis for O and a cc-pVDZ for H in OpenMolcas version 22.06.^{S2} The active space comprised 7 electrons in 5 orbitals (full valence active space) and was averaged over six electronic states. The calculated PECs are depicted in Fig. S1. The dashed blue lines represent the original diabatic PECs of $X^2\Pi$ and $A^2\Sigma^+$ fitted by Korolkov and Paramonov,^{S1} while the dotted green lines show our fit of the $1^2\Sigma^-$ and $1^2\Delta$ states. Note that the original PECs by Korolkov and Paramonov do not perfectly match the RMS-CASPT2 curves, as their minima are lower in energy. Fitting all the states based on the RMS-CASPT2 curves would be the most consistent approach, yet we wished to keep the parametrization of the lowest two states by Korolkov and Paramonov^{S1} since we built on top of their work by using pulses tuned for their PECs. Hence, we fitted only the two dissociative states and added them to the Hamiltonian designed by Korolkov and Paramonov. Although not fully consistent with the RMS-CASPT2 calculations, this description of the potential energy curves preserves the original parametrization, and we note that the PECs are adequately described in the dissociation limit. Once again, we emphasize that our four-state model is only intended to preserve the main features of the potential energy curves of the OH radical.

The diabatic couplings were set to zero between all the electronic states. This approximation might appear as strong, noticing the crossing of the $A^2\Sigma^+$ and $1^2\Sigma^-$ electronic states. However, the calculations with RMS-CASPT2 in the adiabatic representation showed a practically zero energy gap at the crossing point between these two electronic states, suggesting a negligible diabatic coupling. Zero diabatic couplings also mean that the adiabatic states preserve their shape, yet they are energy-ordered such that they never cross.

The transition dipole moment (TDM) between the two lowest electronic states used by Korolkov and Paramonov is shown in the right panel of Fig. S1. Our RMS-CASPT2 calculations revealed that all TDMs between the ground electronic state and excited states share similar shapes and magnitudes, while the TDMs between excited states are negligible. Although the TDM fitted by Korolkov and Paramonov has almost double the magnitude and a different shape compared to the RMS-CASPT2 calculations, we decided to keep it as the laser pulses tuned in their work use this TDM. We took the RMS-CASPT2 calculation as inspiration and used the same parametrization for the TDMs between the ground state and the other excited states.

Finally, we provide below the Molcas input file used for generating the PECs.

```
/*RMS-CASPT2 OH radical calculation */
```

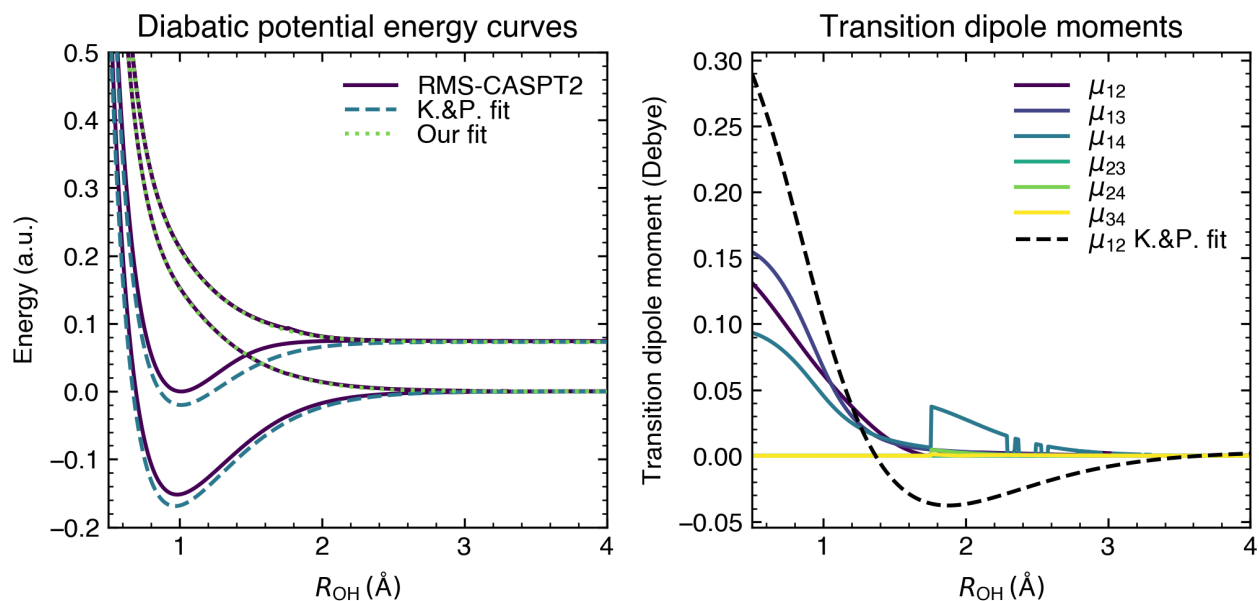


Figure S1: Left Panel: Diabatic potential energy curves of the OH radical calculated at the RMS-CASPT2 level of theory (solid violet lines). The fits by Korolkov and Paramonov^{S1} (dashed blue lines) and our fit for the dissociative curves based on the RMS-CASPT2 potentials (dotted green lines) are included as well. Right Panel: Transition dipole moments calculated at the RMS-CASPT2 level of theory (solid) and the fit proposed by Korolkov and Paramonov^{S1} (dashed) for these quantities.

```

&GATEWAY
  Coord=oh.xyz
  Basis=0.cc-PVTZ,H.cc-PVDZ
  Group=Nosym

&SEWARD

&SCF
  UHF
  Charge=0
  Spin=2

&RASSCF
  nactel = 7 0 0
  inactive= 1
  ras2 = 5
  spin = 2
  ciroot = 6 6 1

```

```
&CASPT2
  rmultistate=6 1 2 3 4 5 6
  MAXIter=50
  properties
```

```
&RASSI
  Heff
  TDMN
  1.0D-20
```

2 Quantum dynamics within a truncated basis of vibronic states

We present additional quantum-dynamics simulations using a truncated basis of vibronic states and compared them to the results presented in the main text (Fig. S2). Panels A (seven vibronic states facilitating full population transfer) and D (two-vibronic-state model with largely underestimated population transfer) are featured in the main text, and panels B and C will be discussed here. Fig. S2B and Fig. S2C show the effect of adding off-resonant vibrational states to only one of the electronic states considered. While both cases bring significant improvement over the simple two-vibronic-state model, neither of them results in a full population transfer. These results highlight that off-resonant vibrational states in both electronic states are necessary to fully capture the photoexcitation dynamics.

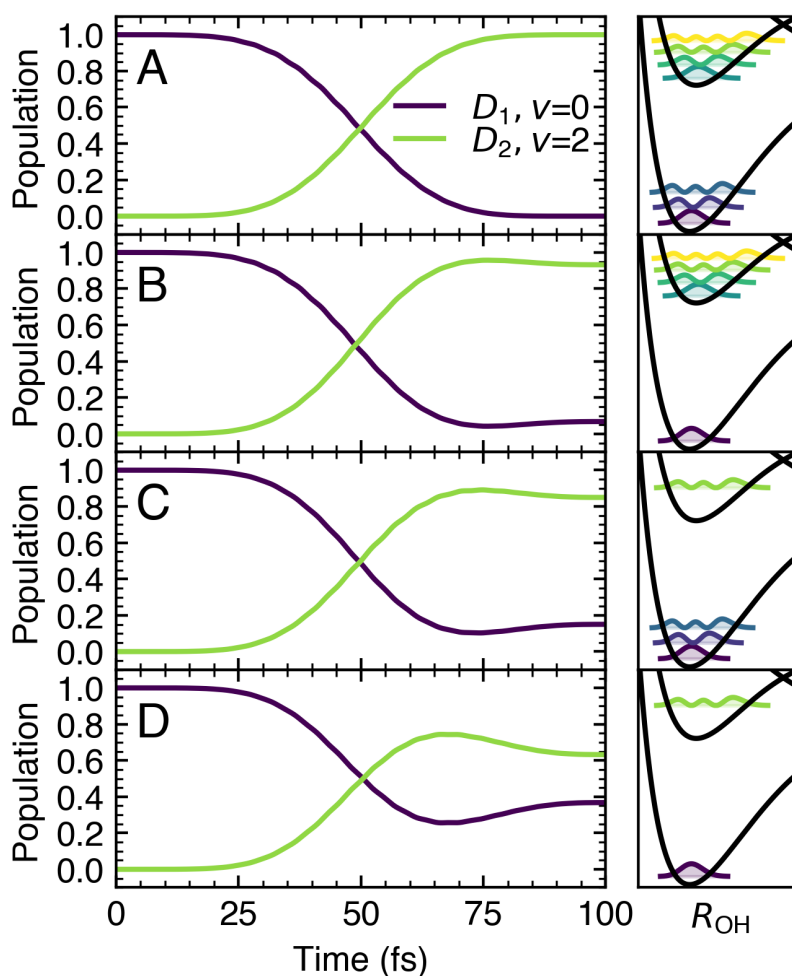


Figure S2: Populations of the $|D_1, v = 0\rangle$ (purple) and $|D_2, v = 2\rangle$ (green) states resulting from quantum-dynamics simulations with a truncated expansion of vibronic states: **A** seven vibronic states (three in D_1 , four in D_2), **B** five vibronic states (one in D_1 , four in D_2), **C** four vibronic states (three in D_1 , one in D_2), **D** two vibronic states (one in D_1 , one in D_2). The vibrational eigenstates used in the expansion are depicted in the right panels.

3 Decomposition of the TD PES into its gauge-dependent and gauge-independent components, and test of different gauges

We provide here a detailed analysis of the EF quantities during photoexcitation dynamics of the OH radical. The TD PES can be split into a gauge-dependent (GD) and a gauge-independent (GI) part as

$$\varepsilon(R, t) = \varepsilon_{\text{GI}}(R, t) + \varepsilon_{\text{GD}}(R, t), \quad (1)$$

where

$$\varepsilon_{\text{GD}}(R, t) = -i\hbar \langle \Phi(R, t) | \frac{\partial}{\partial t} | \Phi(R, t) \rangle_r, \quad (2)$$

$$\varepsilon_{\text{GI}}(R, t) = \langle \Phi(R, t) | \hat{H}_{\text{el}} + \hat{V}_{\text{int}}^e(\mathbf{r}, t) | \Phi(R, t) \rangle_r + \frac{\langle \nabla \Phi(R, t) | \nabla \Phi(R, t) \rangle_r}{2M} - \frac{A^2(R, t)}{2M}. \quad (3)$$

The EF dynamics presented in the main text for the 100-fs and 1-fs pulses used a gauge where the vector potential is set to zero [$A(R, t) = 0$], and the components of the resulting TD PES are presented in Figs. S3 and S4. The very same quantum dynamics is then expressed in the EF using a different gauge where the nuclear phase is now set to zero [$S(R, t) = 0$], see Figs. S5 and S6. Note that in this zero-nuclear-phase gauge, the nuclear dynamics are governed not only by TD PES but also by the vector potential. Hence, the dynamics cannot be interpreted using only TD PES, but also the vector potential, which represents the nuclear momentum field, must also be accounted for.

Note that for the dynamics resulting from a photoexcitation with the 100-fs pulse, both choices of gauge result in quantitatively similar dynamics for the TD PES. Hence, the gauge choice appears negligible in this case, and the same dynamics would be observed even for multidimensional cases where the zero-vector-potential gauge is not possible, and the zero-nuclear-phase gauge is typically used instead. The similarity of results from both gauges is not surprising, considering that the system features minimal momentum during the dynamics, and the vector potential is, therefore, negligible. An animation for the quantum dynamics within the zero-nuclear-phase gauge is available using the following [link](#). For the dynamics associated to a photoexcitation with the 1-fs laser pulse, we observe that the TD PES behaves differently within the two gauges tested, especially when the laser pulse is over. At 5.5 fs and in the zero-nuclear-phase gauge (Fig. S6), the regions of TD PES supporting the split nuclear wave function are not separated by a barrier as in the zero-vector-potential gauge case, but by a step. The difference between the two gauges emerges from the momentum of the dissociating wave packet, which gives rise to a significant vector potential in the zero-nuclear-phase gauge. Hence, both TD PES and the vector potential are necessary for the interpretation of the dynamics. Animation for the zero-nuclear-phase gauge dynamics is available using the following [link](#).

3.1 100-fs pulse in the zero-vector-potential gauge

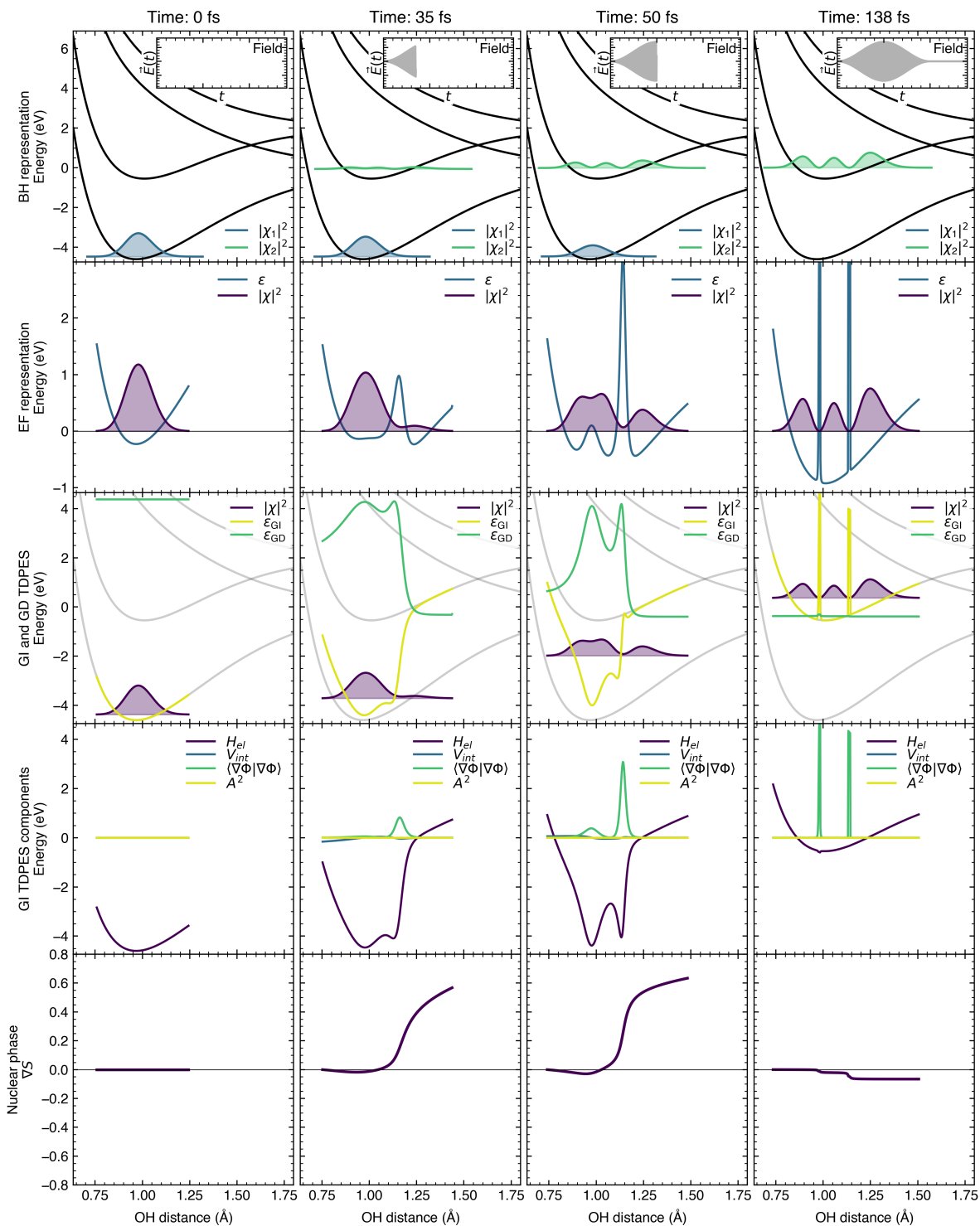


Figure S3: Decomposition of EF quantities for the photoexcitation of OH radical triggered by a 100-fs pulse in the zero-vector-potential gauge. Animation of the dynamics is available using the following [link](#).

3.2 1-fs pulse in the zero-vector-potential gauge

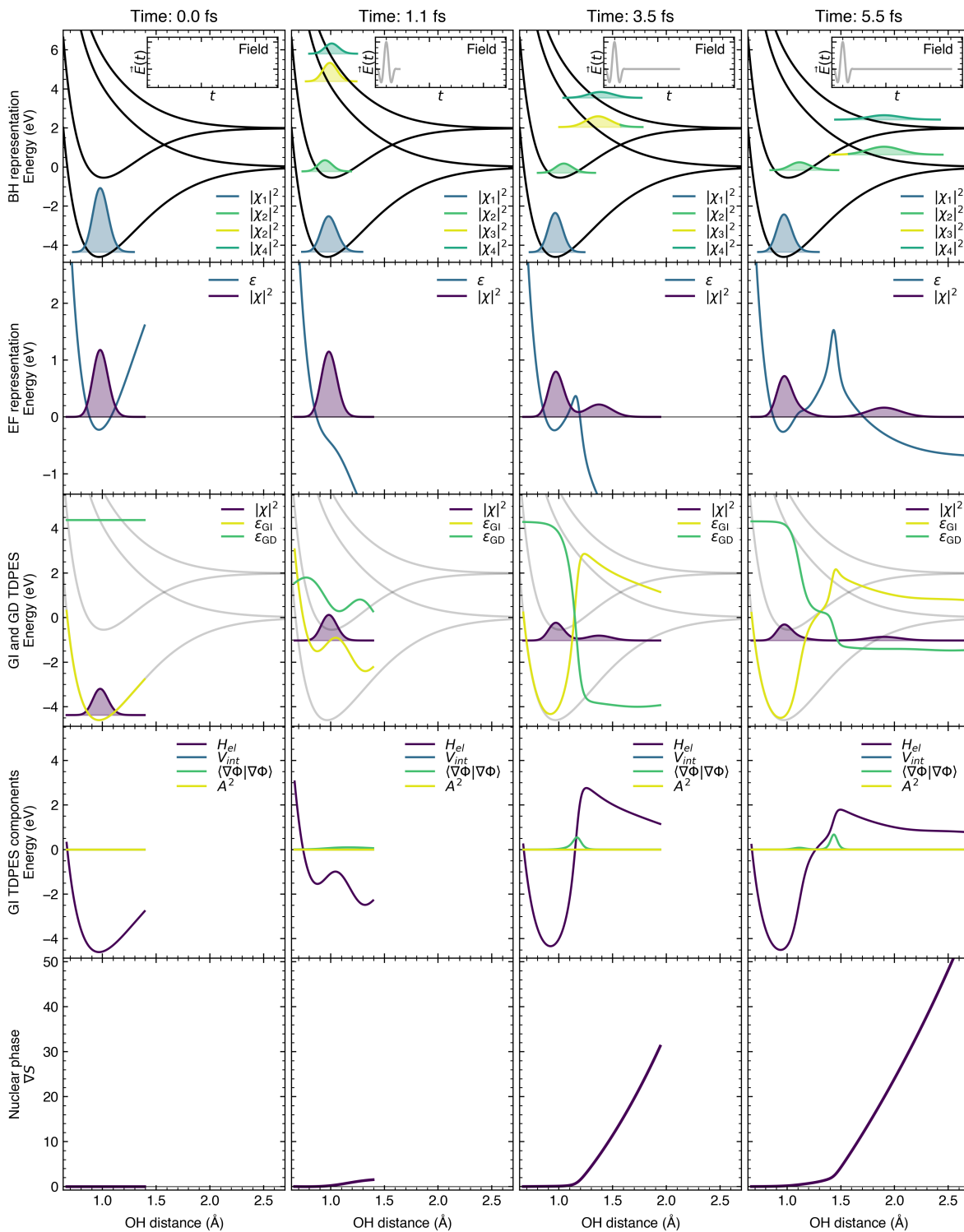


Figure S4: Decomposition of EF quantities for the photoexcitation of OH radical triggered by a 1-fs pulse in the zero-vector-potential gauge. Animation of the dynamics is available using the following [link](#).

3.3 100-fs pulse in the zero-nuclear-phase gauge

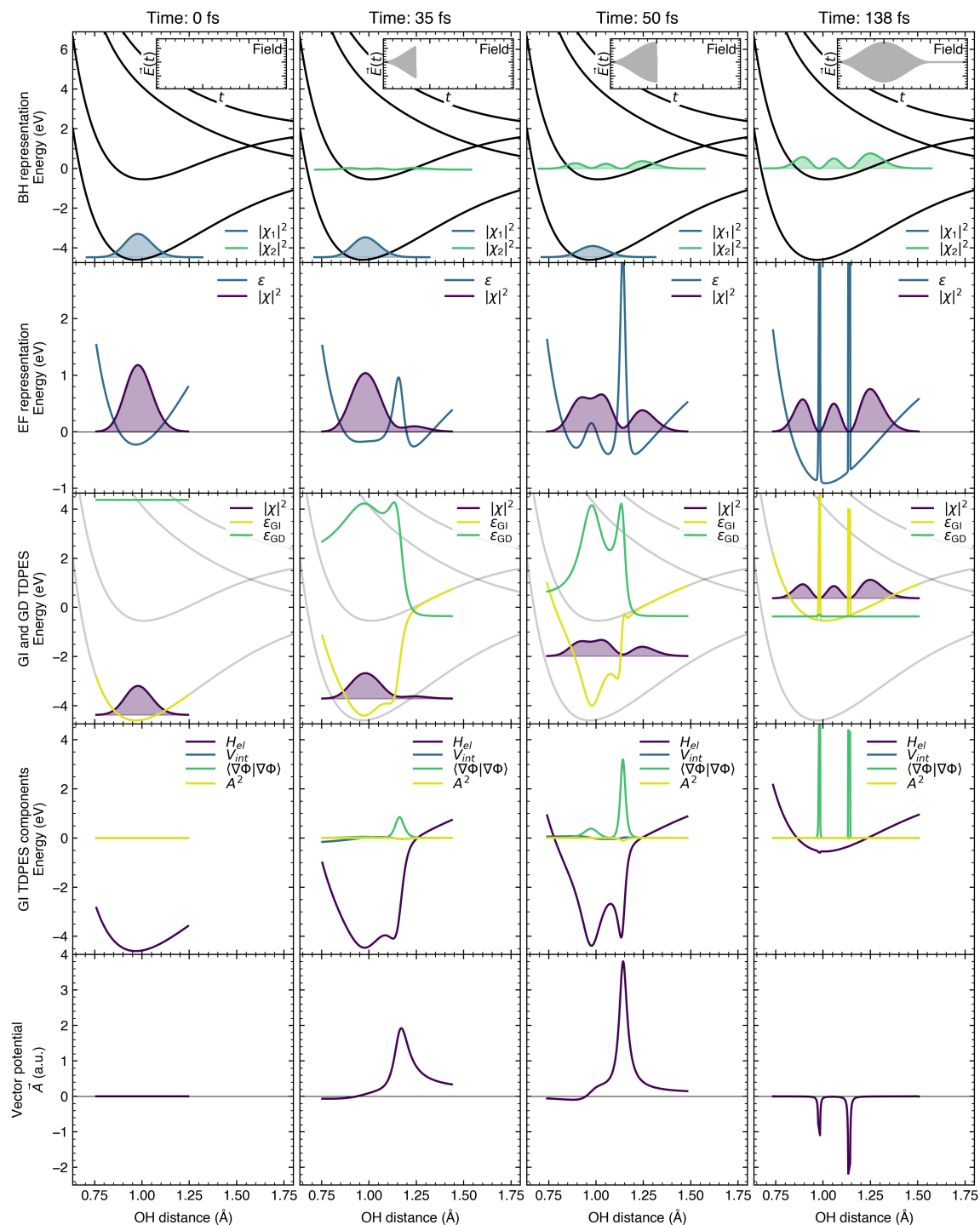


Figure S5: Decomposition of EF quantities for the photoexcitation of OH radical triggered by a 100-fs pulse in the zero-nuclear-phase gauge. Animation of the dynamics is available using the following [link](#).

3.4 1-fs pulse in the zero-nuclear-phase gauge

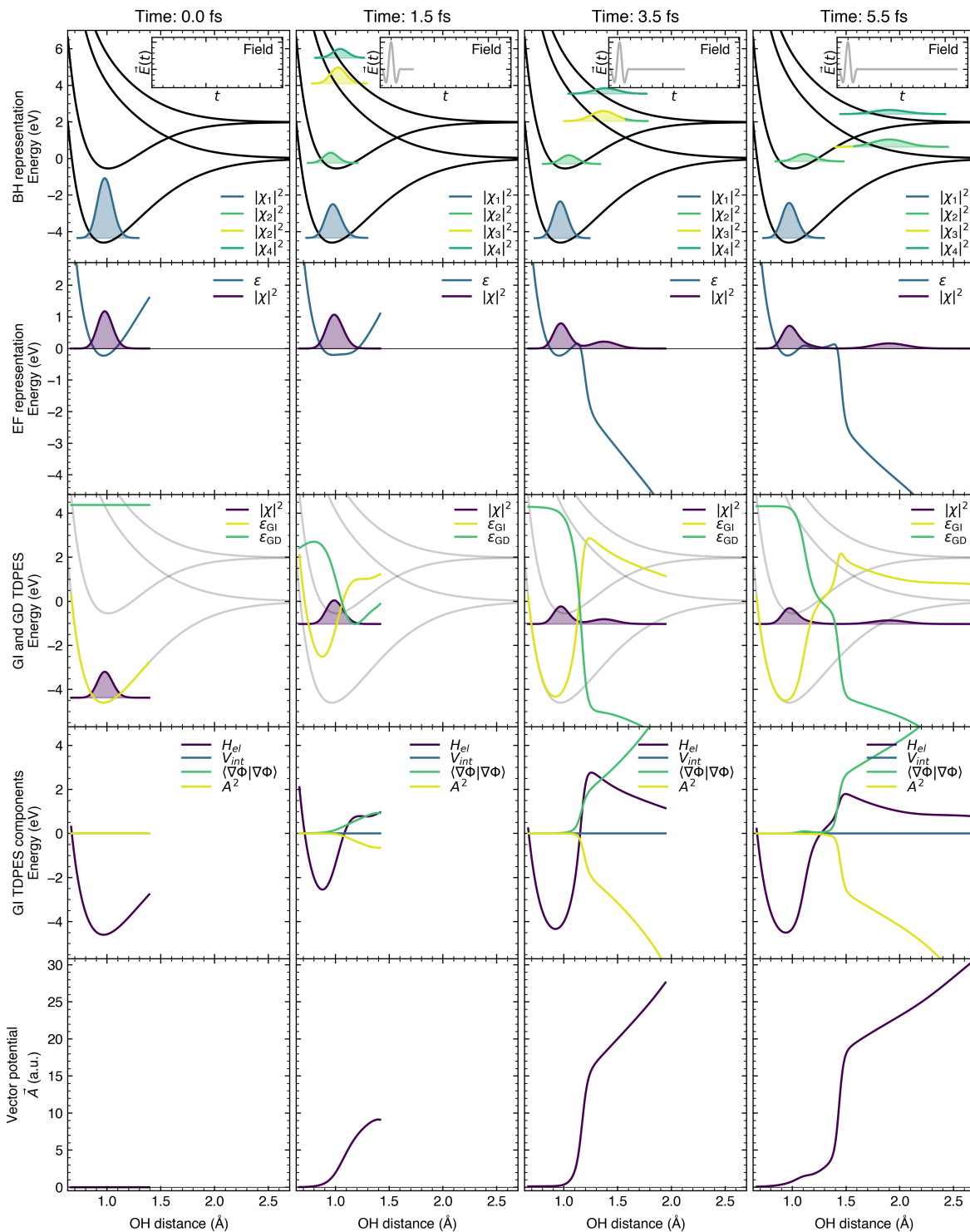


Figure S6: Decomposition of EF quantities for the photoexcitation of OH radical triggered by a 1-fs pulse in the zero-nuclear-phase gauge. Animation of the dynamics is available using the following [link](#).

References

- (S1) Korolkov, M. V.; Paramonov, G. K. Vibrationally state-selective electronic excitation of diatomic molecules by ultrashort laser pulses. *Physical Review A - Atomic, Molecular, and Optical Physics* **1998**, *57*, 4998–5001.
- (S2) Li Manni, G.; Fdez. Galván, I.; Alavi, A.; Aleotti, F.; Aquilante, F.; Autschbach, J.; Avagliano, D.; Baiardi, A.; Bao, J. J.; Battaglia, S.; Birnoschi, L.; Blanco-González, A.; Bokarev, S. I.; Broer, R.; Cacciari, R.; Calio, P. B.; Carlson, R. K.; Carvalho Couto, R.; Cerdán, L.; Chibotaru, L. F.; Chilton, N. F.; Church, J. R.; Conti, I.; Coriani, S.; Cuéllar-Zuquin, J.; Daoud, R. E.; Dattani, N.; Decleva, P.; de Graaf, C.; Delcey, M. G.; De Vico, L.; Dobrutz, W.; Dong, S. S.; Feng, R.; Ferré, N.; Filatov, M.; Gagliardi, L.; Garavelli, M.; González, L.; Guan, Y.; Guo, M.; Hennefarth, M. R.; Hermes, M. R.; Hoyer, C. E.; Huix-Rotllant, M.; Jaiswal, V. K.; Kaiser, A.; Kaliakin, D. S.; Khamesian, M.; King, D. S.; Kochetov, V.; Krośnicki, M.; Kumaar, A. A.; Larsson, E. D.; Lehtola, S.; Lepetit, M. B.; Lischka, H.; López Ríos, P.; Lundberg, M.; Ma, D.; Mai, S.; Marquetand, P.; Merritt, I. C.; Montorsi, F.; Mörchen, M.; Nenov, A.; Nguyen, V. H. A.; Nishimoto, Y.; Oakley, M. S.; Olivucci, M.; Oppel, M.; Padula, D.; Pandharkar, R.; Phung, Q. M.; Plasser, F.; Raggi, G.; Rebolini, E.; Reiher, M.; Rivalta, I.; Roca-Sanjuán, D.; Romig, T.; Safari, A. A.; Sánchez-Mansilla, A.; Sand, A. M.; Schapiro, I.; Scott, T. R.; Segarra-Martí, J.; Segatta, F.; Sergentu, D. C.; Sharma, P.; Shepard, R.; Shu, Y.; Staab, J. K.; Straatsma, T. P.; Sørensen, L. K.; Tenorio, B. N. C.; Truhlar, D. G.; Ungur, L.; Vacher, M.; Veryazov, V.; Voß, T. A.; Weser, O.; Wu, D.; Yang, X.; Yarkony, D.; Zhou, C.; Zobel, J. P.; Lindh, R. The OpenMolcas Web: A Community-Driven Approach to Advancing Computational Chemistry. *Journal of Chemical Theory and Computation* **2023**, *19*, 6933–6991.